Fall 2018

# Characterization of Particulate Matter Accumulated on Ramalina farinacea in the Seattle Area Using Semi-Automated Electron Microscopy

Tor G. (Tor Gunnar) Guddal
*Western Washington University*, theothergunnar@gmail.com

### Recommended Citation

# Characterization of Particulate Matter Accumulated on *Ramalina farinacea* in the Seattle Area Using Semi-Automated Electron Microscopy

By

Tor Gunnar Guddal

Accepted in Partial Completion
of the Requirements for the Degree
Master of Science

ADVISORY COMMITTEE

Dr. Ruth Sofield, Chair

Dr. Robin Matthews

Dr. Troy Abel

GRADUATE SCHOOL

Dr. Gautam Pillay, Dean

**Master's Thesis**

In presenting this thesis in partial fulfillment of the requirements for a master's degree at Western Washington University, I grant to Western Washington University the non-exclusive royalty-free right to archive, reproduce, distribute, and display the thesis in any and all forms, including electronic format, via any digital library mechanisms maintained by WWU.

I represent and warrant this is my original work, and does not infringe or violate any rights of others. I warrant that I have obtained written permissions from the owner of any third party copyrighted material included in these files.

I acknowledge that I retain ownership rights to the copyright of this work, including but not limited to the right to use all or part of this work in future works, such as articles or books.

Library users are granted permission for individual, research and non-commercial reproduction of this work for educational purposes only. Any further digital posting of this document requires specific permission from the author.

Any copying or publication of this thesis for commercial purposes, or for financial gain, is not allowed without my written permission.

Tor Gunnar Guddal

November 26, 2018

**Characterization of Particulate Matter Accumulated
on *Ramalina farinacea* in the Seattle Area Using
Semi-Automated Electron Microscopy**


A Thesis
Presented to
The Faculty of
Western Washington University



In Partial Fulfillment
Of the Requirements for the Degree
Master of Science



by
Tor Gunnar Guddal
November 2018

# Abstract

Semi-automated scanning electron microscopy (SEM) with energy-dispersive X-ray spectroscopy (EDS) can be used to determine the size and composition of filtered particulate matter (PM). This information is valuable for determining the identity and contribution of overlapping air emissions. One limitation of this method is the cost of filtering PM at enough locations to give meaningful spatial data. To address this limitation, I developed an exploratory method to collect PM using *Ramalina farinacea* for semi-automated SEM analysis as a component of lichen biomonitoring studies. I applied this method as a proof of concept in the Seattle area to better understand trends in regional urban dust. To do this, bags of lichen were transplanted to 9 locations in the Duwamish Valley and adjacent uplands for 3 months between September and December, 2017. Some of these locations were arranged close to major industrial sources of airborne metals, which we hypothesized would contribute to the PM observed on the lichens alongside the regional background signature of particulate emissions. Upon collection, PM deposition on the lichen was characterized using SEM with EDS. A total of 18,581 particles were identified and analyzed using the PACLA for Oxford two-stage classifier. My findings suggest that *R. farinacea* are an effective tool for collecting PM and show the greatest proportion of anthropogenic-specific particles on lichens adjacent to Interstate 5. Furthermore, the spatial trends of PM between locations suggest that fugitive dust controls such as green walls and green spaces may be more effective than point source controls at further reducing exposure to harmful dust in the Seattle area.

**Keywords:** Seattle air quality, lichen biomonitoring, semi-automated scanning electron microscopy, particulate matter, urban dust

# Acknowledgments

**Table of Contents**

## List of Tables and Figures

# Introduction

## Background

### Study Objectives

I designed this study to test an exploratory air quality monitoring method involving single particle characterization of particles accumulated on the surface of lichens. The first objective of this study was to develop a method for lichen deployment, collection, and surface particle characterization for source apportionment. The second objective was to apply this method as a proof of concept in the Seattle area to evaluate the composition, spatial distribution, and sources of particulate emissions in and upland of the Duwamish Valley. I hypothesized that the chemical composition of particles accumulated on the lichens at each location would reflect the influence of both regional background and nearby emission sources.

### Overview of Airborne Particulates

Particulate matter (PM), which includes aerosolized liquids, ultrafine dust, biological dust, and secondary aerosols, is one of the six criteria air pollutants regulated by the EPA under the Clean Air Act (C.F.R. 40 § 50 1998, US EPA 2018a). Particulate emissions are regulated based on aerodynamic diameter ($d_a$), which is defined as the diameter of a hypothetical perfect sphere with the same settling rate as a given irregular particle. These include $PM_{10}$ ($d_a \leq 10$ μm) and $PM_{2.5}$ ($d_a \leq 2.5$ μm; C.F.R. 40, § 50.6 2006). Typically, $PM_{10}$ penetrates the thoracic cavity 3 cm below the trachea in humans, and $PM_{2.5}$ penetrates the nonciliated airspace at the terminus of the tracheobronchial tree, although exact penetration depths for $PM_{10}$ and $PM_{2.5}$ depend on breathing patterns and the individual (Stahlhofen et al. 1980, Heyder et al. 1986).

The nonciliated airspace has an especially thin epithelium that promotes gas exchange, which leads to greater solubility and absorption of PM (Lippmann 1977). Additionally, larger

and insoluble particles trapped in the nonciliated airway may be retained for years until removed via mucociliary transport. Together, these factors represent potential for a much greater length of exposure for $PM_{2.5}$ compared to $PM_{10}$. Upon exposure, the primary cause of toxicity for PM is from abrasion and inflammation of soft tissue in the lungs and circulatory system, which leads to heart disease, asthma, and bronchitis from restricted air and blood flow (Brunekreef and Holgate 2002).

Regulation has emphasized PM mass, rather than specific sources, in part due to a World Health Organization (WHO) air quality guideline. The guideline concluded that, although biological response was linked to the chemical properties of PM, there was not enough evidence in the literature that urban PM had significantly altered toxicity between different cities or compared to PM generated from biomass combustion despite different chemical compositions (WHO 2006). This was later supported by an integrated science assessment by the US EPA (2009). A review of literature conducted by Cassee et al. (2013), as a part of WHO (2013), concluded that recent work has begun to show increased evidence that PM toxicity is influenced by source and chemical composition but emphasized the need for additional research.

Sources of PM can be natural or anthropogenic. Natural PM includes wildfire ash, volcano and lightening debris, sea spray precipitates, and crustal dust from aeolian erosion (Calvo et al. 2013). Crustal PM can also be associated with anthropogenic activities when soil and minerals are disturbed by human activity such as mining, eroding asphalt, or tilling a field. Common PMs that can only be sourced from anthropogenic activities (anthropogenic-specific PM) include soot, fly ash, and wear particles from manufacturing, smelting, coal combustion, vehicle exhaust, brakes, and tires (Thorpe and Harrison 2008, Abbasi et al. 2013, Calvo et al. 2013). All of these sources generate PMs with specific compositional and morphological

signatures that are often unique to their sources. These signatures can be used for receptor modeling to identify major contributors to air pollution in regions with multiple, overlapping emissions (Cooper and Watson 1980). Receptor modeling, which models sources using observed PM distribution, is used in contrast to dispersion modeling, which models PM distribution using observed sources.

*PM Monitoring Overview*

Particulate matter collection methods can be divided into continuous and discrete samplers. Continuous samplers involve rapid, often destructive, methods to achieve high-resolution temporal data for a single metric, such as size using beta-attenuation, or mass using a tapered element oscillating microbalance. Typically, continuous samplers offer better temporal data than discrete samplers.

Discrete sampling collects PM using techniques such as air filters or sedimentation on adhesive surfaces. These methods require little to no electricity and oversight during collection, which makes them an affordable option compared to continuous sampling for high resolution spatial data. Additionally, the PM is preserved in discrete sampling, which can be analyzed with more informative methods such as gravimetric, isotopic composition, and single particle analysis.

Single particle analysis offers advantages over other analytical methods by including geometric or chemical composition information for individual particles. This leads to a more representative source characterization than other methods which composite all particles in a sample into their average mass or composition. There are many analytical methods capable of single particle analysis, including time-of-flight mass spectrometry (Pastor et al. 2003), Raman microscopy (Rosasco et al. 1975, Craig et al. 2017), inductively coupled plasma mass

spectrometry (Kawaguchi et al. 1986), scanning electron microscopy (SEM) with energy dispersive x-ray spectroscopy (EDS) (Willis et al. 2002), and others reviewed by Elmes and Gasparon (2017).

Single particle SEM-EDS can be manual, computer controlled (CCSEM), or semi-automated (Willis et al. 2002). Manual SEM-EDS involves user-guided SEM operation and manually recorded observations. In CCSEM, stage movement, image calibration, and data collection are all automated to collect a mosaic of images or series of EDS observations. Semi-automated SEM-EDS is another method in which the data collection can be automated, but image settings must be calibrated by hand for each observation field. The chemistry and morphology data from any of these single particle SEM-EDS approaches can be statistically analyzed with a range of models including hierarchical sorting (e.g. Mamane et al. 2010), rule-based classification (e.g. Campos-Ramos et al. 2009, Weinbruch et al. 2010), artificial neural networks (e.g. Xie et al. 1994), and principal components analysis with clustering (e.g. Genga et al. 2012, González et al. 2016).

Meier et al. (2018) used a hybrid statistical analysis for single particle SEM-EDS in which particles were first described using rule-based classification, and then divided into subclasses using cluster analysis. This results in a very large number of subclasses, which enables more confident source attribution because each subclass represents a more restrictive set of characteristics. In addition, this approach creates a library of particles that can be standardized and compared between studies.

*Lichen Biomonitoring*

Although biological effects were not reported in my study, one of the goals of the project was to establish methods and exposure information for future particle analysis as an extension of lichen

biomonitoring programs. Biomonitoring is useful as a low-cost method for evaluating environmental conditions, and as a direct way to determine biological effect where other, nonbiological, monitoring methods ignore contextual factors such as bioavailability and toxicity of the monitored substance. Donovan et al. (2016) is a prominent regional example of biomonitoring that used moss to identify previously unknown cadmium emissions in Portland. Donovan et al. (2016) showcased the value of biomonitoring as an exploratory tool by using an extensive low-cost sampling grid to identify two anomalous emission sources without needing to design a study around a specific chemical or location.

Lichens, a complex of algae or cyanobacteria and ascomycete fungi, are valuable in biomonitoring for their responsiveness to atmospheric pollutants due to their nonvascular, epiphytic, autotrophic characteristics (Garty 2001). Their extensive interaction with and heavy reliance on the atmosphere for energy, nutrients, and water makes bioaccumulation of metals in lichens an effective predictor of bulk deposition from urban and natural dust (Jenkins and Davies 1966, Saeki at al. 1977, Andersen et al. 1978). Bioaccumulation in lichen has been used for both spatial mapping to predict emission magnitude (Donovan et al. 2016) and receptor modeling to predict emission sources (Landis et al. 2012, Boamponsem et al. 2017). In addition to bioaccumulation, lichen have been applied to environmental monitoring using oxidative stress biomarkers (Cuny et al. 2004, Oztetik and Cicek 2011), community composition (Branquinho et al. 1999), and collecting PM for single particle SEM-EDS.

Early single particle SEM-EDS with lichen used manual SEM-EDS to characterize individual particles as part of bioaccumulation studies (Garty et al. 1979, Johnsen 1981, Olmez 1985). More recently, Williamson et al. (2004) used semi-automated SEM-EDS with a rule-based classifier on the lichen *Hypogymnia physodes* adjacent to a copper smelter. Mróz et al.

(2018) used Antarctic moss and lichen to detect extraterrestrial dust, demonstrating the use of single particle SEM-EDS for low-concentration particulates. Each of these studies benefited from opportunistic sampling using either preexisting lichen that had been collecting PM over the course of their lifetime, or lichen that had been deployed as part of a larger biomonitoring program.

*Study Area*

The study region spans across the Duwamish Valley and adjacent uplands in parts of Burien and South Seattle in King County, Washington (Figures 1-3, Appendix A). The Duwamish Valley is home to some of the largest emitters of metals into the air in Washington State (Table 1; US EPA 2018b) and elevated airborne metals compared to surrounding areas (King County 2015), resulting in a disproportionate effect on low-income communities, especially near freeways (Bae et al. 2007). The northern end of the Duwamish Valley contains the Seattle Industrial District, Harbor Island, the neighborhoods Georgetown and South Park, and the King County International Airport/Boeing Field, as well as lowland sections of Delridge (Figure 1). The eastern edge of the northern Duwamish Valley is bordered by Interstate 5 and the Beacon Hill neighborhood, and the western edge is bordered by the North Admiral and Delridge neighborhoods in South Seattle.

The climate in the study region was mild throughout the sampling period of September 25 through December 21, 2017. Average monthly temperature ranged from -1.2°C in December to 15.4°C in September, and average monthly precipitation ranging from 3.4 cm in September to 22.5 cm in November (NOAA 2018). There were 23 days during the sampling period with windspeeds below 5 mph, pressure above 30 "Hg, and scattered to no clouds (Time and Date AS 2018), which can lead to temperature inversions. The longest consecutive period of such

conditions lasted ten days from December 4 to December 14. Wind in Seattle generally blows from the south and southeast during the time of year which my study took place (Natural Resources Conservation Service, 2003).

Twelve industrial facilities in the study region reported air releases of metals in their Toxics Release Inventory (TRI) reports in 2017 (Table 1, Figure 2; US EPA 2018b). The TRI program is a self-reported database of chemical releases mandated by the Emergency Planning and Community Right-to-Know Act of 1986 and Pollution Prevention Act of 1990 for businesses with over ten employees in specific industries that use over a certain threshold of TRI-listed chemicals. Of the 12 TRI reporting facilities in the study region in 2017, the majority of metal emission weight, based on total metals reported, were in the northern Duwamish Valley with 62% north of Georgetown in the Industrial District and Harbor Island, 21% in Georgetown, and 17% in South Park. Ace Galvanizing and Ardagh Glass accounted for 91% of Georgetown and South Park air emissions with 1500 lbs. zinc released in 2017 by Ace Galvanizing 470 lbs. chromium and 1143 lbs. lead released by Ardagh Glass. Facilities north of Georgetown in the Duwamish Valley reported a total of 5774 lbs. of copper, zinc, chromium, manganese, nickel, lead, aluminum, and mercury in 2017 (Table 1).

Additional, unaccounted, emissions in the study region include mobile sources, wildfire smoke, and residential emissions. These are not reported as a part of the TRI program. Mobile sources include flights taking off and landing at Boeing field and automobiles. Highway emissions are largely composed of aluminum, barium, iron, potassium, and silicon, as well as carbon, nitrates, and sulfates (US EPA 2018c). Additionally, extreme wildfires in California and Montana during September and October 2017 could have contributed PM, although most of the smoke had dispersed from the study region by the start of monitoring (NOAA 2018).

Anthropogenic contributions to background emissions were also expected from miscellaneous residential sources in the Beacon Hill and North Admiral neighborhoods.

Several receptor modeling studies have been conducted to understand emissions in the Seattle area using the Interagency Monitoring of Protected Visual Environments station at Beacon Hill (Maykut et al. 2003, Kim et al. 2004, Wu et al. 2007). Each of these studies consistently found heavy influence of wood smoke, secondary aerosols, and diesel emissions, with mixed influence from marine, paper processing, metal processing, and soil emissions. In another study, Corey et al. (2006) verified the toxicity of the Beacon Hill PM measured in Maykut et al. (2003) using heart rate variability in mice.

**Study Design**

I selected nine locations for monitoring air emissions in the Seattle area using the lichen *Ramalina farinacea* (Figure 3, Table 2). These included six within the Duwamish Valley (DV1-DV6; numbered from north to south) and one each upland from the Duwamish Valley in a Beacon Hill residential area, North Admiral on the Cleveland High School (CHS) campus, and adjacent to Interstate 5 (U1-U3, respectively). The Duwamish Valley locations were arranged in pairs near Ace Galvanization in Georgetown, Ardagh Glass in South Park, and Sound Propeller between South Park and Glendale. The upland locations were used for a comparison to regional residential and highway emissions. A subsample of lichens that were not deployed (PD) were used to characterize pre-deployment conditions. I hypothesized that lichen would accumulate PM corresponding to known emission sources near each of the locations. To do this, I used *R. farinacea* as a low-cost PM collection media for semi-automated SEM-EDS analysis and the two-stage classification model, PACLA for Oxford, described in Meier et al. (2018).

## Materials and Methods

### Biomonitoring

The lichen *R. farinacea* used for this study grows between 30-60° N on the North American coast (Bowler and Rundel 1978). It was selected for the smooth, branching, thallus which should be suitable for collecting particles for SEM-EDS observation, as well as for being native to the study region. Furthermore, the broad morphology of *R. farinacea* was considered beneficial to biomonitoring due to the high surface to volume ratio and rugged surface characteristics (Garty 2001).

The lichen collection and biomonitoring strategy was developed using guidance from Stolte et al. (1993), Geiser (2004), and Ares et al. (2012). In my study, approximately 200 g *R. farinacea* were collected on September 25, 2017 from live woody branches on the west face of Sehome Arboretum in Bellingham, Washington (Figure 1). These were taken from the interior of Sehome Arboretum to limit exposure to urban PM sources. The lichens were hand-picked clean of debris and rinsed using 1 L Ultrapure water per 100 g material. Excess water was removed with a centrifugal dryer at 45 × g for 10 seconds and by air-drying the lichens overnight. The lichens were placed in 10 cm × 22 cm nylon pouches with 3 mm mesh size that were divided into three compartments, each with approximately 1.3 g of lichen. Each of these compartments was defined as a subsample throughout this study. A galvanized wire was threaded through the bottom of the bags for stability, to retain the orientation of the sampler, and to move water accumulated on the nylon pouches away from the lichens (Figure 4). The lichen bags were stored at -10˚C for three days until deployment. Additional pre-deployment lichens (PD) were stored at -10˚C throughout the entire study.

Two lichen bags were suspended in each of nine locations across the Seattle area on September 29 and 30, 2017 (Figure 3, Table 2). The Duwamish Valley (DV) locations were arranged in pairs within 400 m of Ardagh Glass (DV1 and DV2), Sound Propeller (DV3 and DV4), or Ace Galvanization (DV5 and DV6; Figure 2). Lichen bags were also deployed in three locations uplands (U1-U3) of the Duwamish Valley. Location U1 was next to the CHS greenhouse, which was unused during the study period, between the staff parking lot and 15th Ave South. Cleveland High School is located in a residential neighborhood about 120 m uphill from Interstate 5 separated by a green wedge. Location U2 was deployed in a residential neighborhood in North Admiral, about 1.2 km away from the nearest industrial land use and 2.3 km away from the nearest TRI reporting facility. Location U3 is adjacent to the CHS Playfield, approximately 8 m from an Interstate 5 on-ramp and 120 m from location U1. The distances between each location and nearby TRI reporting facilities were evaluated using the Pasquill-Gifford air dispersion model to ensure that the predicted emission trajectories would pass low enough to intercept the lichens (Hanna et al. 1977).

The lichen bags were strung at a mean height of 2.7 m above the ground with a minimum of 3 m distance from roadways and 10 cm from buildings (Figure 4, Table 2). The height, distance from buildings, and qualitative exposure to sun, drip, air flow, vehicle, and industrial influences were noted at the initial deployment and second retrieval (December 21, 2017) for each location, and latitude, longitude, elevation, and distance to roads were calculated later using Google Maps (2018; Table 2). The qualitative estimates were all described on a scale of one to five and averaged when features changed between visits. Sun exposure was determined by estimating unobstructed sky to the south between 8° and 30° altitude angle. Drip exposure was described by the amount of visible overhead sky. Air flow was estimated based on relative

distance to the nearest obstruction in any horizontal direction. Industrial influence was estimated based on land use and TRI data within visible distance of each location.

The bags were retrieved from all locations on October 13 and December 21, 2017 (18 and 87 days of deployment) and stored at 0˚C. A preliminary assessment of particle counts was conducted with SEM and it was determined that the December 21 samples would be better for semi-automated SEM-EDS because the October 13 samples did not have enough particle accumulation. The October 13 samples were not used in this study but were used in another study to investigate metal accumulation in the whole lichen (Johnson et al. in prep) using inductively coupled plasma mass spectrometry (ICP-MS; Branquinho et al. 1999, Søndergaard 2013). The October 13 samples will not be considered further in this thesis.

**Sample Analysis**

*Particle Identification and Characterization*

Branching segments of lichen from each subsample (nine locations plus the pre-deployment lichens with three subsamples each; n = 30) were dried in a desiccator and mounted on aluminum SEM mounts for imaging using carbon tabs and a 60 second gold/palladium coating. On each subsample, two 183 μm by 244 μm observation fields (n = 60) were randomly selected for imaging from the interior edge of the upper cortex where *R. farinacea* branches and collects the highest density of particulates (Figure 5). Additional observation fields were used when the first contained less than 100 particles, and different observation fields were used when PM was obscured by too many particles or an irregular lichen substrate. New lichen branches were mounted twice when an entire branch was ineligible for particle analysis based on these criteria.

Semi-automated SEM-EDS analysis of PM was conducted using Oxford AZtec feature mapping on a JEOL JSM-7200F Field Emission SEM with backscatter detector and Oxford X-

Max$^N$ 150 EDS detector according to manufacturer and laboratory specifications adjusted for

lichen (Table 3). The chemical analysis was semi-quantitative and normalized to 100% to

account for the uneven surface of the PM, which does not allow for a complete ZAF correction.

Particles smaller than 0.5 μm or with a mean atomic weight similar to carbon were not counted

or analyzed. The background signature of the coated lichen was determined by scanning clear

regions of cortex and found to be a median of 63% carbon and 41% oxygen with an upper 99%

percentile of 2.66% gold from the coating and 0.22% potassium, with no other elements detected

after deconvolution. Due to the background signature of lichens, all carbon and oxygen, and

elements present with concentrations less than 5% were treated as 0% composition, and the

remaining elements were recalculated to 100% composition (Meier et al. 2018). Periodic

validation of the semi-automated SEM-EDS was conducted during the microscopy by reviewing

the composition of several particles to verify they contained realistic elemental ratios for crustal

and anthropogenic PM.

*Exploratory Endpoints*

I explored usnic acid (Stark et al. 1950, Caviglia et al. 2001), glutathione (Smith et al. 1988),

malondialdehyde (Wills 1964, Boutin et al. 1998), thallus coloration, and chlorophyll

degradation (Ronen and Galun 1984, Arar 1997) as biomarkers of lichen health. All of these

failed to pass quality control criteria, possibly because of the chemical variations between

chemotypes of *R. farinacea* (Bowler and Rundel, 1978), which were not measured in this study.

Analysis of the biomarkers have been omitted from further analysis in this thesis.

**Statistical Analysis and Modeling**

*Data Treatment with Two-Stage Classifier*

The particles were grouped into classes, subclasses, and source classes by the PACLA for

Oxford classifier which was developed and run with my data by Particle Vision GmbH in

TOWN NAME, Switzerand (Meier et al. 2008; Version 180302). The first stage of the model

used a rule-based classifier to group particles composed of the same elements into classes. The

second stage of the model grouped particles into subclasses based on similarity to a library of

particle composition clusters. The particle composition cluster library was developed using

geologic reference material and field sampling from anthropogenic sources such as automotive,

railway, and metal and slag recycling. Subclasses were assigned a source class when the

composition cluster was consistently associated with a single source from the particle library

such as mineral or brake wear.

*Descriptive Statistics*

All statistical analysis was conducted using RStudio with the core, fmsb, plyr, psych, ternary,

and viridis packages (Wickham 2011, R Core Team 2017, Allaire 2017, Smith 2017, Garnier

2018, Nakazawa 2018, Revelle 2018, RStudio Team 2016). Rank based statistics were used for

all analysis unless otherwise noted because the data failed to meet assumptions of normality or

homoscedasticity. Subsamples within each location were pooled and treated as six observation

fields per location because there was not enough statistical power to describe the variance

between the subsamples at each location.

Pairwise correlations within classes and subclasses at each location were conducted using

Kendall's Tau on the classes and subclasses that were present in at least 80% of the locations. A

random, linear, amount of noise between -0.0001 and 0.0001 was added to each class and

subclass at each location to resolve ties. Corrections for repeated measures were not made due to the large number of comparisons. Pairwise Kendall's Tau correlations were also conducted for the source classes, but none yielded significant results ($\alpha = 0.05$).

*Location Comparisons*

Variance between the subclass frequencies at each location were compared using principal component analysis (PCA) with one of each correlated pairs of subclasses removed (Kendall's Tau, $\alpha = 0.01$), and the remaining subclasses centered and scaled. The locations were then hierarchically clustered by Euclidean distance across the least number of components using Ward's method from the ward.D2 function in R Studio (Ward 1963, Murtagh and Legendre 2014). The strongest eight positive and eight negative variable loadings were used to display notable similarities and differences between locations with star plots. This clustering was also repeated using only the subclasses present in at least 80% of the locations to determine whether the trends were dependent on sparse data.

## Results and Discussion

**Electron Microscopy**

*Sampling Considerations*

The upper cortex topography under SEM was typically either smooth, rough, or very rough, and curved or planar (Figures 6 and 7). Particle composition was easily observed on smooth and rough surfaces and was obscured or out of focus on especially rough or curved surfaces. Additionally, observation fields on the lichen that had extremely high particle density would cause particles to obscure each other and merge their chemical and morphological signature (Figure 7). I was able to avoid all issues encountered with lichen surface topography by selecting new observation fields or by using a new lichen from the same location.

*Electron Microscopy of Particles*

A total of 18,581 particles were observed on the lichen (Supplementary Material A). Periodic review of particle composition always showed realistic element ratios for crustal and anthropogenic PM; therefore, the semi-automated SEM-EDS analysis passed the validation criteria. The particles were commonly angular, clustered, irregular, oblong, polymineralic, rough, or spheroid (Figure 8). Spheroid and oblong are the only particles that were identifiable by their geometric parameters. Clustered and polymineralic particles were identified, but not distinguished from other particles, and may have led to skewed particle counts (Figure 9). This is because different regions of clustered and polymineralic particles fall above and below feature recognition threshold on the SEM, so the centers were counted as a single particle and fragments were occasionally counted as one or more distinct particles. This can be considered an over or under estimation of particle counts depending on whether the clustered and polymineralic

particles are recorded by the SEM-EDS software as a single, fragmented, particle or several

distinct particles clustered together.

Particles that were expected to be indistinguishable from the background lichen signal

using semi-automated SEM-EDS with PACLA for Oxford include plastic, nonmetal tire wear,

and soot (Rausch 2018). Using manual identification, a single particle of soot was found

(Figure 9). This is substantially less than the approximately 25% of combustion products found

on Beacon Hill using filters in Maykut et al. (2003), Kim et al. (2004), and Wu et al. (2007),

which suggests an artifact of sample design in my study such as rain, sample height, or lichen

physiology blocked or removed soot from the lichen surface. The absence of the reported

chromium and lead from locations DV1 and DV2 is also notable, given the presence of these

metals in Ardagh Glass emissions. This indicates these metals were either taken up by the lichen

via solubilization (Burgstaller et al. 1993), absorbed into the thallus (Garty 2001), failed to reach

the lichen entirely, or were below the size cutoff of 0.5 µm.

*Summary Statistics*

Lichen particle density ranged from 851 to 15,363 particles/mm$^2$, with a median of 6,707

particles/mm$^2$. No location had significantly greater particle density than any other location

(Figure 10; Kruskal-Wallis, $\alpha = 0.05$). This lack of difference is because the procedure used to

select which sections of a subsample to analyze was biased against lichens with very low and

very high particle density.

The aerodynamic diameter, which is typically smaller than particle width, of observed

particles ranged from 0.4 to 49.5 µm, with a median of 1.70 µm across (Figure 11). Of the

particles analyzed, 93% were PM$_{10}$, and 50% were PM$_{2.5}$. No location showed significantly

different sized particles than the others (Kruskal-Wallis, $\alpha = 0.05$). Particle composition roughly

follows what should be expected from mixed crustal and biologic sources except for the approximately 4% of entirely iron particles which can be generally attributed to anthropogenic sources (Figure 12). The individual particle data is included as a supplementary file (Supplementary Material A.csv), available through CEDAR (WWU) Associated Files.

**PACLA for Oxford Particle Classifier**

*PM classes and subclasses*

A total of 358 classes, 509 subclasses, and 10 sources were identified using the PACLA for Oxford classifier (Appendix B, Supplementary Material B). The number of particles in both classes and subclasses ranged from 1 to 1,875 particles, with a median of 3 particles. Approximately 81% of all particles were classified to a subclass, and 65% were classified to a source class. Of these, 88 classes and 141 subclasses contain at least 10 particles. The most complex class was Si.Al.Ca.K.Ti.Fe.Cl.S.P with 9 components, and the most complex class containing at least 10 particles was Si.Al.Ca.Mg.Ti.Fe, with 6 components. There were highly significant correlations between 15 pairs of classes and 36 pairs of subclasses ($\alpha = 0.01$; Table 4 and 5). Each of these correlations represented a probable shared natural or anthropogenic source.

The absence of an NaCl class was notable because Kim et al. (2010) and Maykut et al. (2003) each reported 12% source contribution of sea salt to South Seattle PM. The absence in my particles may be due to moisture in the lichens, which would dissolve the salt during deployment and storage. Classes for chromium, lead, and zinc were also unaccountably missing from the locations adjacent to Ace Galvanization and Ardagh Glass (DV1, DV2, DV4, and DV6). Possible explanations include too small of particle size for detection, the metals being distributed below detection level in a large number of particles, sampling while the facilities were not emitting these metals, inaccurate TRI reporting, or the particles being solubilized or absorbed

into the lichen. Environmental factors such as rain dissolving or flushing particles off the lichen are also possible reasons for not finding chromium, lead, and zinc; although, no significant correlations were found between any subclass and relative sun, overhead drip, or air flow exposure (Kendall's Tau, $\alpha = 0.05$). This supports our assumption that environmental factors had a negligible influence on particle class abundance in our sampling program.

*PM Sources*

The PM source classes can be grouped by crustal and anthropogenic-specific sources when describing location trends (Table 6; Figure 13). Included in the crustal sources are calcite, marl, mineral, quartz, and soil. The anthropogenic-specific sources identified include tire, brake, and vehicle-industrial. Location U3 had the greatest density of all anthropogenic source classes, containing 34% of all observed anthropogenic-specific particles. Locations PD, DV4, and U1 contained 11%, 15%, and 18% of all anthropogenic-specific particles, respectively, and the other locations each contained less than 10% of anthropogenic-specific particles. Location U2 contains a low proportion of anthropogenic-specific sources, which supports the use of U2 to represent the regional background signature of PM. It should be emphasized that the model cannot distinguish crustal PMs suspended by anthropogenic activity from those transported through natural mechanisms.

Of the crustal sources observed, similar amounts of minerals appeared within the DV1-DV4 locations. The predominance of soil particles in DV5 and DV6 may be attributed to proximity to less developed areas with more trees and grass. The increase in marl and calcite at DV3 can be explained by DV3 being the only location adjacent to gravel roads, which often contain limestone and other Ca-rich materials (Snellings et al. 2012). Even so, the 5.3% of Ca-rich material at DV3 was similar to the average of 4.3% found in the Xie et al. (2005) semi-

automated SEM-EDS study of urban dust, and much lower than the 25.7% Ca-rich particles found in the Mamane et al. (2001) CCSEM study of urban dust.

Anthropogenic-specific sources were found at all locations, but U3 is characterized by a much greater proportion of brake, vehicle-industrial, and tire particles than the others. There was also some mineral, quartz, and marl at U3 which can be explained by intensified road wear from heavy and high-speed vehicles on Interstate 5. The U1 location roughly resembled the source signature of U3, but with less mineral, tire, and vehicle-industrial particles (Figure 13), indicating that these sources had a greater association with heavy or high-speed vehicles. Additionally, the increased proportion of brake particles at U1 could indicate a measurable shift in emissions adjacent to the reduced speed in parking lots and school zones. This was supported by DV5, the only other location with a strong brake signal, being the only location immediately adjacent to a traffic light. Additionally, the low proportion of anthropogenic-specific particles across the Duwamish Valley locations (DV1-DV6) suggests that emission controls are succeeding in reducing the emissions that can be detected using semi-automated SEM-EDS on lichen, or that deployed lichens do not capture all of the particles.

*Multivariate Location Comparisons*

Hierarchical clustering of the first four components of the subclass PCA was used to cluster the locations. This revealed two clusters, with locations DV5 and DV6 grouped together, and locations DV3, DV4, U1, U2, and PD together (Figures 14-18). Locations DV1, DV2, and U3 did not cluster with any other source and were considered outliers. This suggested that the DV5 and DV6 locations had unique influences from the others, and the DV3, DV4, U1, and U2 locations did not vary significantly from pre-deployment conditions (PD). The similarity to pre-deployment conditions could be caused by either low particle deposition during the study period,

or from a particle equilibrium where new particles similar to the pre-deployment particles were deposited on the lichen just as fast as pre-deployment particles were solubilized or otherwise lost. The strongest factors influencing the PCA scores were (Table 7):

- Si.Al.Ca.Mg.K.Fe.Cl.S_0 (unknown source)

- Si.Al.Ca.Ba.Fe.S_0 (unknown source)

- Si.Al.Ca.Na.Fe.S_1 (mineral source)

- Si.Al.Ca.K.Fe.S_3 (mineral source)

- Si.Al.Ca.K.P_0 (unknown source)

Removing the subclasses that appear on less than 80% of the locations shifted the variance to the first three components and caused the locations to cluster poorly (Table 8; Figures 19 and 20). This indicated that the driving factors of location similarities were infrequent particles.

**Conclusions and Future Directions**

*Using Lichen for Semi-Automated SEM*

The data obtained from the semi-automated SEM-EDS analysis of PM on *R. farinacea* were successfully used with the PACLA for Oxford particle classifier. The automation of PM observation is an improvement on the work of Garty et al. (1979), Johnsen (1981), and Olmez (1985), which were limited by the number of particles that could be observed with manual SEM. Weinbruch et al. (2010) also used semi-automated analysis for biological monitoring of PM but was limited by the structural stability of moss for PM observation. By using the broad structure of *R. farinacea*, I was able to overcome this limitation and automate the collection of a large number of particles. Williamson et al. (2004) used a similar approach to my own, which was further improved upon with updated SEM-EDS and particle classification methods from Meier et al. (2018). Incorporating the PACLA for Oxford classifier with biological single particle SEM-EDS monitoring enabled the classification of the expansive number of particles that I was able to collect with the low-cost, automated, sampling procedure. Because of this, I recommend *R. farinacea* as an opportunistic PM sampler during biomonitoring studies to characterize PM exposure alongside established methods for testing biological effects.

The value of lichens for PM collection came with several limitations. One such limitation was the inability to identify low-atomic weight particles such as carbonaceous clusters. This is a limitation of most substrates used in PM collection, which are also carbon-based, but work with boron substrates has enabled identification of carbonaceous particles and may surpass carbon substrates, along with lichen, in their use (Choël et al. 2005). Another limitation is the possibility of the lichen solubilizing or otherwise dispersing some particles, as suggested by the lack of sea salt precipitates in my study which were observed in Maykut et al. (2003) and Kim et al. (2004).

Accounting only for the insoluble particles may be a hinderance for source apportionment studies but can also be framed as an advantage for studies interested in biologically relevant particles. For example, Mills et al. (2008) found that ambient maritime PM did not cause the same magnitude of inflammation that an equivalent mass of urban PM was known to cause, meaning that the absence of NaCl on the lichen could represent a more accurate characterization of the biologically relevant PM in the study area, although a controlled study would be needed to confirm this hypothesis.

Future work with the lichen would benefit from controlled PM exposure or side-by-side deployment with discrete monitoring stations to understand the interactions between lichens and particles on their surface. Additionally, this work would benefit from a fully automated method of SEM-EDS that could pass over regions with poor topography or too many particles. It would also be useful to identify a method to distinguish clustered and aggregate particles, which otherwise skew particle counts. Environmental factors such as sunlight and drip exposure did not appear to influence the occurrence of any particle class, although a more robust assessment of environmental factors is needed to confirm this.

*Assessment of Emissions*

An assessment of Seattle region emissions was conducted as a proof of concept for the lichen monitoring method developed in my study. As such, limitations of the method are largely unexplored and should be addressed in future work. Using this method, I found that emissions in the study area were driven by both anthropogenic-specific and crustal PM. Location U3 at the CHS Playfield near Interstate 5 was the only area dominated by anthropogenic-specific emissions, while the releases of chromium, lead, and zinc from Ace Galvanization and Ardagh Glass were not apparent from my sampling methods. The unobserved PM from Ace Galvanizing

and Ardagh Glass suggest that stack emissions in the region were successfully dispersed throughout the atmosphere during the study period despite favorable conditions for temperature inversions. Because stack emissions were not concentrated in the valley, fugitive dust controls such as green walls and green spaces may be more successful in controlling emissions than additional point source regulation. This is further supported by the dissimilarity between locations U1 and U3 even though the two were only separated by a 120 m distance and a green wedge.

The observed distributions of PMs differ from the receptor modeling conducted for Beacon Hill in Maykut et al. (2003) and Kim et al. (2004) which found approximately 60-80% industrial influence and 6-14% soil influence for the particles detectable with my method. In contrast, I found 18% industrial and 57% crustal particles at the U1 location near the Maykut et al. (2003) and Kim et al. (2004) sampling station on Beacon Hill, and similar or larger proportions of crustal material at the other sampling locations. This may be attributed to differences in how sources are estimated in each model and from differences in sampling methods. Further investigation into these differences could be used to highlight strengths and weaknesses of both methods for source apportionment.

These conclusions come with several limitations, including the possibility that some particles were solubilized or absorbed into the lichen, flushed off from rainfall, present as minor fractions of other particles but below detection limits, too small to detect, or that the emissions missed the lichens entirely due to wind, air flow, or interaction with the materials used for suspending the lichen. In addition, my method cannot estimate total suspended particles or bulk deposition because particle coverage was not consistent across each lichen, so it is possible that PM from the adjacent industrial facilities was present but masked by ambient PM from road dust

and emissions not reported in the TRI program. Many of these limitations could be further investigated using a greater spatial distribution of lichen bags, year-round sampling, and paired nonbiological passive samplers.

Another limitation of this method is preexisting particulates on the lichens. Typical single-particle SEM-EDS studies have used filters to collect PM so that any PM observed can be attributed to the study region. Harvesting lichen for PM collection means that PM was already embedded into the lichen tissue despite cleaning procedures. To address this, I characterized initial PM using the PD lichens and described the final PM as a shift from initial conditions. This revealed that four of the Duwamish Valley locations shifted towards a smaller proportion of crustal PM than observed on the PD lichens (Table 6). It is possible that the sample location on Sehome Hill had greater anthropogenic influences than the deployment locations, although this is doubtful given the magnitude of difference in reported emissions between the Seattle area and Bellingham. Rather, I believe the high proportion of anthropogenic-specific particles on PD were caused by the combined effect of two factors. First, many of the subclasses were attributed to unknown sources and crustal material. A large fraction of unaccounted anthropogenic influence could have come from these unknown source classes and masked the anthropogenic signal in the Duwamish Valley. Second, the Duwamish Valley is drier and dustier than Sehome Hill where the lichens were collected, which will have exaggerated the proportion of crustal sources and suppressed the influence of anthropogenic-specific sources. Regardless of whether there was preexisting anthropogenic influence on the lichen, I expected some degree of PM replacement on the lichen surface during the deployment period, which would have reduced the influence of preexisting PM on the lichen.

Limitations of this work should continue to be investigated, but the method nevertheless represents a novel approach to PM monitoring that should be further explored. The successful application of this method in Seattle as a proof of concept provides an exciting, practical approach that compliments existing biological and non-biological monitoring networks.

## Literature Cited

Abbasi, S., Jansson, A., Sellgren, U., & Olofsson, U. (2013). Particle emissions from rail traffic: a literature review. *Critical reviews in environmental science and technology*, 43(23), 2511-2544.

Allaire, J.J., Wickham, H., Ushey, K., & Ritchie., g (2017). Rstudioapi: safely access the RStudio API. R package version 0.7.

Andersen, A., Hovmand, M. F., & Johnsen, I. B. (1978). Atmospheric heavy metal deposition in the Copenhagen area. *Environmental Pollution*, 17(2), 133-151.

Arar, E. J. (1997). Determination of chlorophyll a and b and identification of other pigments of interest in marine and freshwater algae using high performance liquid chromatography with visible wavelength detection. *Methods for the Determination of Chemical Substances in Marine and Estuarine Environmental Matrices*, 447, 1-20.

Ares, A., Aboal, J. R., Carballeira, A., Giordano, S., Adamo, P., & Fernández, J. A. (2012). Moss bag biomonitoring: a methodological review. *Science of the Total Environment*, 432, 143-158.

Bae, C. H. C., Sandlin, G., Bassok, A., & Kim, S. (2007). The exposure of disadvantaged populations in freeway air-pollution sheds: a case study of the Seattle and Portland regions. *Environment and Planning B: Planning and Design*, 34(1), 154-170.

Boamponsem, L. K., de Freitas, C. R., & Williams, D. (2017). Source apportionment of air pollutants in the Greater Auckland Region of New Zealand using receptor models and elemental levels in the lichen, Parmotrema reticulatum. *Atmospheric Pollution Research*, 8(1), 101–113.

Boutin, A.C., Shirali, P., Garçon, G., Gosset, P., Leleu, B., Marez, T., Bernard, A. & Haguenoer, J.M. (1998, January). Peripheral markers (clara cell protein and α-glutathione S-transferase) and lipidoperoxidation (malondialdehyde) assessment in Sprague-Dawley rats instilled with haematite and benzo [a] pyrene. In *Journal of Applied Toxicology* 18(1), 39-45.

Bowler, P. A., & Rundel, P. W. (1978). The *Ramalina farinacea* complex in North America: chemical, ecological and morphological variation. *Bryologist*, 386-403.

Branquinho, C., Catarino, F., Brown, D. H., Pereira, M. J., & Soares, A. (1999). Improving the use of lichens as biomonitors of atmospheric metal pollution. *Science of the Total Environment*, 232(1-2), 67-77.

Brunekreef, B., & Holgate, S. T. (2002). Air pollution and health. *The Lancet*, 360(9341), 1233-1242.

Burgstaller, W., & Schinner, F. (1993). Leaching of metals with fungi. *Journal of Biotechnology*, 27(2), 91-116.

Calvo, A. I., Alves, C., Castro, A., Pont, V., Vicente, A. M., & Fraile, R. (2013). Research on aerosol sources and chemical composition: past, current and emerging issues. *Atmospheric Research*, 120, 1-28.

Campos-Ramos, A., Aragón-Piña, A., Galindo-Estrada, I., Querol, X., & Alastuey, A. (2009). Characterization of atmospheric aerosols by SEM in a rural area in the western part of México and its relation with different pollution sources. *Atmospheric Environment*, 43(39), 6159-6167.

Cassee, F. R., Héroux, M. E., Gerlofs-Nijland, M. E., & Kelly, F. J. (2013). Particulate matter beyond mass: recent health evidence on the role of fractions, chemical constituents and sources of emission. *Inhalation Toxicology*, 25(14), 802-812.

Caviglia, A. M., Nicora, P., Giordani, P., Brunialti, G., & Modenesi, P. (2001). Oxidative stress and usnic acid content in *Parmelia caperata* and *Parmelia soredians* (Lichenes). *Il Farmaco*, 56(5-7), 379-382.

Choël, M., Deboudt, K., Osán, J., Flament, P., & Van Grieken, R. (2005). Quantitative determination of low-Z elements in single atmospheric particles on boron substrates by automated scanning electron microscopy-energy-dispersive x-ray spectrometry. *Analytical Chemistry*, 77(17), 5686-5692.

Cooper, J. A., & Watson Jr, J. G. (1980). Receptor oriented methods of air particulate source apportionment. *Journal of the Air Pollution Control Association*, 30(10), 1116-1125.

Corey, L. M., Baker, C., & Luchtel, D. L. (2006). Heart-rate variability in the apolipoprotein E knockout transgenic mouse following exposure to Seattle particulate matter. *Journal of Toxicology and Environmental Health, Part A*, 69(10), 953-965.

Craig, R. L., Bondy, A. L., & Ault, A. P. (2017). Computer-controlled Raman microspectroscopy (CC-Raman): A method for the rapid characterization of individual atmospheric aerosol particles. *Aerosol Science and Technology*, 51(9), 1099-1112.

Cuny, D., Van Haluwyn, C., Shirali, P., Zerimech, F., Jérôme, L., & Haguenoer, J. M. (2004). Cellular impact of metal trace elements in terricolous lichen *Diploschistes muscorum* (Scop.) R. Sant.–identification of oxidative stress biomarkers. *Water, Air, and Soil Pollution*, 152(1-4), 55-69.

Donovan, G. H., Jovan, S. E., Gatziolis, D., Burstyn, I., Michael, Y. L., Amacher, M. C., & Monleon, V. J. (2016). Using an epiphytic moss to identify previously unknown sources of atmospheric cadmium pollution. *Science of the Total Environment*, 559, 84-93.

Elmes, M., & Gasparon, M. (2017). Sampling and single particle analysis for the chemical characterisation of fine atmospheric particulates: A review. *Journal of Environmental management*, 202, 137-150.

Garnier, S. (2018). Viridis: Default Color Maps from 'matplotlib'. R package version 0.5.1.

Garty, J. (2001). Biomonitoring atmospheric heavy metals with lichens: theory and application. *Critical Reviews in Plant Sciences*, 20(4), 309-371.

Garty, J., Galun, M., & Kessel, M. (1979). Localization of heavy metals and other elements accumulated in the lichen thallus. *New Phytologist*, 82(1), 159-168.

Geiser, L. (2004). Manual for monitoring air quality using lichens on national forests of the Pacific Northwest. US Department of Agriculture-Forest Service, Pacific Northwest Region, Air resource Management.

Genga, A., Baglivi, F., Siciliano, M., Siciliano, T., Tepore, M., Micocci, G., Tortorella, C. & Aiello, D. (2012). SEM-EDS investigation on PM10 data collected in Central Italy: Principal component analysis and hierarchical cluster analysis. *Chemistry Central Journal*, 6(S2), S3.

Google Maps. (2018). Bellingham and Seattle, Washington. Retrieved November 5, 2018 from www.google.com/maps/@47.8012127,-121.561257,8.54z.

González, L.T., Rodríguez, F.L., Sánchez-Domínguez, M., Leyva-Porras, C., Silva-Vidaurri, L.G., Acuna-Askar, K., Kharisov, B.I., Chiu, J.V. & Barbosa, J.A. (2016). Chemical and morphological characterization of TSP and PM2. 5 by SEM-EDS, XPS and XRD

collected in the metropolitan area of Monterrey, Mexico. *Atmospheric Environment*, 143, 249-260.

Hanna, S. R., Briggs, G. A., Deardorff, J., Egan, B. A., Gifford, F. A., & Pasquill, F. (1977). AMS workshop on stability classification schemes and sigma curves—summary of recommendations. *Bulletin of the American Meteorological Society*, 58(12), 1305-1309.

Heyder, J. J. G. C. F. W., Gebhart, J., Rudolf, G., Schiller, C. F., & Stahlhofen, W. (1986). Deposition of particles in the human respiratory tract in the size range 0.005–15 μm. *Journal of Aerosol Science*, 17(5), 811-825.

Jenkins, D. A., & Davies, R. I. (1966). Trace element content of organic accumulations. *Nature*, 210(5042), 1296.

Johnsen, I. B. 1981. Heavy metal deposition on plants in relation to immission and bulk precipitation. *Silva Fennica*,15(4), 444-445.

Johnson, A., Guddal., T.G., Sofield, R.M. (in prep). Untitled.

Kawaguchi, H., Fukasawa, N., & Mizuike, A. (1986). Investigation of airborne particles by inductively coupled plasma emission spectrometry calibrated with monodisperse aerosols. *Spectrochimica Acta Part B: Atomic Spectroscopy*, 41(12), 1277-1286.

Kim, E., Hopke, P. K., Larson, T. V., Maykut, N. N., & Lewtas, J. (2004). Factor analysis of Seattle fine particles. *Aerosol Science and Technology*, 38(7), 724-738.

King County. (2015). Lower Duwamish Waterway Source Control: Supplemental Bulk Atmospheric Deposition Study Final Data Report. Prepared by Jenée Colton, Martin Grassley, and Richard Jack. King County Department of Natural Resources and Parks, Water and Land Resources Division, Science and Technical Support Section. Seattle, Washington.

Landis, M. S., Pancras, J. P., Graney, J. R., Stevens, R. K., Percy, K. E., & Krupa, S. (2012). Receptor modeling of epiphytic lichens to elucidate the sources and spatial distribution of inorganic air pollution in the Athabasca Oil Sands Region. *Developments in Environmental Science*. 11, 427-467.

Lippmann, M. (1977). Regional deposition of particles in the human respiratory tract. *Handbook of Physiology,* 1(9), 213-232.

Mamane, Y., Willis, R., & Conner, T. (2001). Evaluation of computer-controlled scanning electron microscopy applied to an ambient urban aerosol sample. *Aerosol Science & Technology*, 34(1), 97-107.

Maykut, N. N., Lewtas, J., Kim, E., & Larson, T. V. (2003). Source apportionment of PM2.5 at an urban IMPROVE site in Seattle, Washington. *Environmental Science & Technology*, 37(22), 5135-5142.

Meier, M.F., Mildenberger, T., Locher, R., Rausch, J., Zünd, T., Neururer, C., Ruckstuhl, A. & Grobéty, B. (2018). A model based two-stage classifier for airborne particles analyzed with CCSEM. *Journal of Aerosol Science*, 123(2018) 1–16.

Mills, N.L., Robinson, S.D., Fokkens, P.H., Leseman, D.L., Miller, M.R., Anderson, D., Freney, E.J., Heal, M.R., Donovan, R.J., Blomberg, A. & Sandström, T. (2008). Exposure to concentrated ambient particles does not affect vascular function in patients with coronary heart disease. *Environmental Health Perspectives*, 116(6), 709.

Murtagh, F., & Legendre, P. (2014). Ward's hierarchical agglomerative clustering method: which algorithms implement Ward's criterion?. *Journal of classification*, 31(3), 274-295.

Mróz, T., Szufa, K., Frontasyeva, M.V., Tselmovich, V., Ostrovnaya, T., Kornaś, A., Olech, M.A., Mietelski, J.W. & Brudecki, K. (2018). Determination of element composition and extraterrestrial material occurrence in moss and lichen samples from King George Island (Antarctica) using reactor neutron activation analysis and SEM microscopy. *Environmental Science and Pollution Research*, 25(1), 436-446.

Nakazawa, M. (2018). Fmsb: Functions for medical statistics book with some demographic data. R package version 0.6.3.

Natural Resources Conservation Service. (2003). National Water and Climate Center Wind Rose Download. Retrieved October 21, 2018 from www.wcc.nrcs.usda.gov/ftpref/downloads/climate/windrose/washington/seattle/seattle_nov.gif.

NOAA. (2018). National Centers for Environmental information, Climate at a Glance: Statewide Time Series. Published October 2018. Retrieved October 30, 2018 from https://www.ncdc.noaa.gov/cag/

Olmez, Ilhan, M. Cetin Gulovali, and G. E. Gordon. 1985. Trace element concentrations in lichens near a coal-fired power plant. *Atmospheric Environment*, 19(10), 1663-1669.

Oztetik, E., & Cicek, A. (2011). Effects of urban air pollutants on elemental accumulation and identification of oxidative stress biomarkers in the transplanted lichen *Pseudovernia furfuracea*. *Environmental Toxicology and Chemistry*, 30(7), 1629-1636.

Pastor, S. H., Allen, J. O., Hughes, L. S., Bhave, P., Cass, G. R., & Prather, K. A. (2003). Ambient single particle analysis in Riverside, California by aerosol time-of-flight mass spectrometry during the SCOS97-NARSTO. *Atmospheric Environment*, 37, 239-258.

R Core Team (2017). R: A language and environment for statistical computing. R Foundation for Statistical Computing, Vienna, Austria.

RStudio Team (2016). RStudio: Integrated Development for R. RStudio, Inc., Boston, MA. http://www.rstudio.com/.

Rausch, J. (2018, October 9). Personal interview.

Revelle, W. (2018) Psych: Procedures for personality and psychological research. Northwestern University, Evanston, Illinois, USA. R package version 1.8.4.

Ronen, R., & Galun, M. (1984). Pigment extraction from lichens with dimethyl sulfoxide (DMSO) and estimation of chlorophyll degradation. *Environmental and Experimental Botany*, 24(3), 239-245.

Rosasco, G. J., Etz, E. S., & Cassatt, W. A. (1975). The analysis of discrete fine particles by Raman spectroscopy. *Applied Spectroscopy*, 29(5), 396-404.

Saeki, M., Kunii, K., Seki, T., Sugiyama, K., Suzuki, T., & Shishido, S. (1977). Metal burden of urban lichens. *Environmental Research*, 13(2), 256-266.

Smith (2017). Ternary: An R Package for Creating Ternary Plots. R package version 1.0.1.

Smith, I. K., Vierheller, T. L., & Thorne, C. A. (1988). Assay of glutathione reductase in crude tissue homogenates using 5, 5′-dithiobis (2-nitrobenzoic acid). *Analytical Biochemistry*, 175(2), 408-413.

Snellings, R., Mertens, G., & Elsen, J. (2012). Supplementary cementitious materials. *Reviews in Mineralogy and Geochemistry*, 74(1), 211-278.

Stahlhofen, W., Gebhart, J., & Heyder, J. (1980). Experimental determination of the regional deposition of aerosol particles in the human respiratory tract. *American Industrial Hygiene Association Journal*, 41(6), 385-398a.

Stark, J. B., Walter, E. D., & Owens, H. S. (1950). Method of isolation of usnic acid from Ramalina reticulata. *Journal of the American Chemical Society*, 72(4), 1819-1820.

Stolte, K., Mangis, D., Doty, R., Tonnessen, K., & Huckaby, L. S. (1993). Lichens as bioindicators of air quality. United States Department of Agriculture General Technical Report RM-224. Rocky Mountain Forest and Range Experiment Station Fort Collins, Colorado.

Søndergaard, J. (2013). Accumulation dynamics and cellular locations of Pb, Zn and Cd in resident and transplanted Flavocetraria nivalis lichens near a former Pb–Zn mine. *Environmental Monitoring and Assessment*, 185(12), 10167-10176.

Time and Date AS. (2018). 2017 Weather in Seattle. Retrieved November 25, 2018 from www.timeanddate.com/weather/usa/seattle/historic.

Thorpe, A., & Harrison, R. M. (2008). Sources and properties of non-exhaust particulate matter from road traffic: a review. *Science of the Total Environment*, 400(1-3), 270-282.

US EPA. (2009). Integrated Science Assessment (ISA) for Particulate Matter. Retrieved November 5, 2018 from cfpub.epa.gov/ncea/risk/recordisplay.cfm?deid=216546.

US EPA. (2018a). NAAQS Table. Retrieved October 11, 2018 from www.epa.gov/criteria-air-pollutants/naaqs-table.

US EPA. (2018b). TRI Explorer (2017 Dataset (released October 2018)). Retrieved November 25, 2018 from https://www.epa.gov/triexplorer.

US EPA. (2018c). SPECIATE Data Browser, Profile 3261. Retrieved October 20, 2018 from cfpub.epa.gov/speciate/ehpa_speciate_browse_details.cfm?ptype=P&pnumber=3261.

USGS. (2018). National Geospatial Program: The National Map. Retrieved November 1, 2018 from https://viewer.nationalmap.gov/advanced-viewer/.

Ward Jr, J. H. (1963). Hierarchical grouping to optimize an objective function. *Journal of the American Statistical Association*, 58(301), 236-244.

Weinbruch, S., Ebert, M., Gorzawski, H., Dirsch, T., Berg, T., & Steinnes, E. (2010). Characterisation of individual aerosol particles on moss surfaces: implications for source apportionment. *Journal of Environmental Monitoring*, 12(5), 1064-1071.

Wickham, H. (2011). The split-apply-combine strategy for data analysis. *Journal of Statistical Software*, *40*(1), 1-29. R package version 1.8.4.

Williamson, B. J., Mikhailova, I., Purvis, O. W., & Udachin, V. (2004). SEM-EDX analysis in the source apportionment of particulate matter on *Hypogymnia physodes* lichen

transplants around the Cu smelter and former mining town of Karabash, South Urals, Russia. *Science of the Total Environment*, 322(1-3), 139-154.

Willis, R. D., Blanchard, F. T., & Conner, T. L. (2002). Guidelines for the application of SEM/EDX analytical techniques to particulate matter samples. Research Triangle Park (NC 27711, EPA-600/R-02-070).

Wills, E. D. (1964). The effect of inorganic iron on the thiobarbituric acid method for the determination of lipid peroxides. *Biochimica et Biophysica Acta*, 84(4), 475-477.

WHO. (2006). Air quality guidelines: global update 2005. World Health Organization.

WHO. (2013) Review of evidence on health aspects of air pollution – REVIHAAP Project. Retrieved November 5, 2018 from www.euro.who.int/en/health-topics/environment-and-health/air-quality/publications/2013/review-of-evidence-on-health-aspects-of-air-pollution-revihaap-project-final-technical-report

Wu, C. F., Larson, T. V., Wu, S. Y., Williamson, J., Westberg, H. H., & Liu, L. J. S. (2007). Source apportionment of PM2. 5 and selected hazardous air pollutants in Seattle. *Science of the Total Environment*, 386(1-3), 42-52.

Xie, Y., Hopke, P. K., & Wienke, D. (1994). Airborne particle classification with a combination of chemical composition and shape index utilizing an adaptive resonance artificial neural network. *Environmental Science & Technology*, 28(11), 1921-1928.

Xie, R. K., Seip, H. M., Leinum, J. R., Winje, T., & Xiao, J. S. (2005). Chemical characterization of individual particles (PM10) from ambient air in Guiyang City, China. *Science of the Total Environment*, 343(1-3), 261-272.

**Tables**

Table 1. Air releases (lb*yr$^{-1}$) in study area in 2017, ordered by latitude (USEPA, 2018). Region codes are HI = Harbor Island, ID = Industrial District, DR = Delridge, IW = Industrial District West, GT = Georgetown, SP = South Park. The TRI database search was conducted for the 98106, 98108, 98116, 98126, and 98134 zip codes, which covers the study region identified in Figure A1 (Appendix A).

| TRI Facility Report | Code | Latitude | Longitude | Stack Height (m) | Region | Total Metals (lbs.) |
|---|---|---|---|---|---|---|
| ALASKAN COPPER WORKS | AW | 47.575 | -122.326 | 7 | ID | 765 |
| YOUNG CORPORPORATION | YC | 47.573 | -122.351 | 7 | HI | 2510 |
| NUCOR STEEL SEATTLE | NS | 47.569 | -122.367 | 15 | DR | 2468 |
| ASH GROVE CEMENT | AC | 47.568 | -122.343 | 15 | ID | 30.138 |
| LAFARGE NA INC SEATTLE | LN | 47.554 | -122.344 | 16 | IW | 0.6 |
| ARDAGH GLASS | AR | 47.553 | -122.337 | 10 | GT | 1613.1 |
| MOREL INDUSTRIES | MI | 47.553 | -122.325 | 7 | GT | 250 |
| GLACIER NORTHWEST INC | GN | 47.551 | -122.337 | 7 | GT | 0.1 |
| CERADYNE INC A 3M | CI | 47.544 | -122.326 | 6 | GT | 29.2 |
| NON-FERROUS METALS | NM | 47.533 | -122.33 | 5 | SP | 31 |
| SOUND PROPELLER SERVICES | SP | 47.531 | -122.323 | 5 | SP | 9 |
| ACE GALVANIZING | AG | 47.517 | -122.323 | 4 | SP | 1500 |
| Total | | | | | | 9206 |

Table 1. (cont.)

| TRI Facility Report | Code | Stack Emissions (lbs.) | | | | | | | |
|---|---|---|---|---|---|---|---|---|---|
| | | Cr | Cu | Pb | Mn | Hg | Ni | Zn | TOTAL |
| ALASKAN COPPER WORKS | AW | 5 | 5 | | | | 5 | | 15 |
| YOUNG CORPORPORATION | YC | 5 | | | 250 | | 5 | | 260 |
| NUCOR STEEL SEATTLE | NS | 7 | 15 | 184 | 126 | 218 | 3 | 1387 | 1940 |
| ASH GROVE CEMENT | AC | 1.5 | | 1.2 | | 15 | | 12 | 29.7 |
| LAFARGE NA INC SEATTLE | LN | | | 0.3 | | | | | 0.3 |
| ARDAGH GLASS | AR | 470 | | 1143 | | | | | 1613 |
| MOREL INDUSTRIES | MI | | | | | | | | 0 |
| GLACIER NORTHWEST INC | GN | | | 0.1 | | | | | 0.1 |
| CERADYNE INC A 3M | CI | | | 11.4 | | | | | 11.4 |
| NON-FERROUS METALS | NM | | | 27 | | | | | 27 |
| SOUND PROPELLER SERVICES | SP | | | | | | | | 0 |
| ACE GALVANIZING | AG | | | | | | | 750 | 750 |
| Total | | 489 | 20 | 1367 | 376 | 233 | 13 | 2149 | 4647 |

Table 1. (cont.)

| TRI Facility Report | Code | Fugitive Emissions (lbs.) | | | | | | | |
|---|---|---|---|---|---|---|---|---|---|
| | | Cr | Cu | Pb | Mn | Hg | Ni | Zn | TOTAL |
| ALASKAN COPPER WORKS | AW | 250 | 250 | | | | | 250 | 750 |
| YOUNG CORPORPORATION | YC | 750 | | | 750 | | 750 | | 2250 |
| NUCOR STEEL SEATTLE | NS | 143 | 71 | | 207 | | 36 | 71 | 528 |
| ASH GROVE CEMENT | AC | 0.21 | | 0.028 | | | | 0.2 | 0.438 |
| LAFARGE NA INC SEATTLE | LN | | | 0.3 | | | | | 0.3 |
| ARDAGH GLASS | AR | | | 0.1 | | | | | 0.1 |
| MOREL INDUSTRIES | MI | | 250 | | | | | | 250 |
| GLACIER NORTHWEST INC | GN | | | | | | | | 0 |
| CERADYNE INC A 3M | CI | | | 17.8 | | | | | 17.8 |
| NON-FERROUS METALS | NM | | | 4 | | | | | 4 |
| SOUND PROPELLER SERVICES | SP | 5 | | | | | 4 | | 9 |
| ACE GALVANIZING | AG | | | | | | | 750 | 750 |
| Total | | 1148 | 571 | 22 | 957 | 0 | 1040 | 821 | 4559 |

Table 2. Location characterization. Sun, drip, air, vehicle, and industrial were all qualitative scores of observed influences using a scale of 1 to 5. Distance from roads was estimated using labeled streets on Google Maps, which excludes alleys, driveways, and parking lots. Geographic coordinates have been shifted slightly to maintain anonymity. Location codes are DV = Duwamish Valley, U = Uplands, and PD = Pre-deployment. Region codes are GT = Georgetown, SP = South Park, BH = Beacon Hill, NA = North Admiral, and SH = Sehome Hill Arboretum.

| | Latitude | Longitude | Elevation (m) | Height (m) | Sun | Drip | Air Flow | Vehicle | Industrial |
|---|---|---|---|---|---|---|---|---|---|
| DV1 | 47.55161 | -122.335 | 3.0 | 3.7 | 3 | 3 | 4 | 4 | 5 |
| DV2 | 47.55284 | -122.333 | 4.0 | 3.0 | 1 | 1 | 2 | 3 | 4 |
| DV3 | 47.53291 | -122.324 | 4.0 | 2.4 | 1.5 | 4 | 4 | 3 | 2 |
| DV4 | 47.53064 | -122.324 | 3.0 | 4.3 | 1 | 4 | 3.5 | 2 | 2 |
| DV5 | 47.51615 | -122.324 | 16.0 | 1.5 | 1 | 3 | 4 | 4 | 2 |
| DV6 | 47.51675 | -122.323 | 16.0 | 3.4 | 5 | 5 | 5 | 1 | 3 |
| U1 | 47.55114 | -122.314 | 39.0 | 1.2 | 2 | 2 | 2 | 3 | 1 |
| U2 | 47.58860 | -122.389 | 84.0 | 2.1 | 2.5 | 5 | 3.5 | 1 | 1 |
| U3 | 47.55125 | -122.316 | 22.0 | 2.7 | 2.5 | 5 | 3.5 | 5 | 1 |
| PD | 48.73562 | -122.482 | 103.5 | - | - | - | - | - | - |

Table 2. (cont.)

|  | Latitude | Longitude | Hung from | Distance to Roads (m) | Distance to Buildings | Land Use | Region | Other influences |
|---|---|---|---|---|---|---|---|---|
| DV1 | 47.55161 | -122.335 | Industrial shelving | 32 | 50 cm | Industrial | GT | |
| DV2 | 47.55284 | -122.333 | Eaves | 12 | 30 cm | Industrial | GT | |
| DV3 | 47.53291 | -122.324 | Downspout | 22 | 10 cm | Industrial | SP | Gravel roads |
| DV4 | 47.53064 | -122.324 | Chain fence | 10 | 5 m | Industrial | SP | Cigarettes |
| DV5 | 47.51615 | -122.324 | Tree | 3 | 2 m | Industrial | SP | Stoplight |
| DV6 | 47.51675 | -122.323 | Chain fence | 79 | 15 m | Industrial | SP | |
| U1 | 47.55114 | -122.314 | Greenhouse exterior | 15 | 10 m | High School | BH | Parking lot |
| U2 | 47.58860 | -122.389 | Tree | 30 | 5 m | Residential | NA | |
| U3 | 47.55125 | -122.316 | Tree | 9 | 50 m | Highway | BH | |
| PD | 48.73562 | -122.482 | - | 138 | 220 m | Forested | SH | |

Table 3. SEM and EDS settings.

| | |
|---|---|
| Magnification | 500x |
| Scanning Area | 183 μm x 244 μm (0.044652 mm$^2$) |
| Accelerating Voltage | 20 kV |
| Lower Grey Threshold | Calibrated per sample |
| Input Count Rate | 35000 CPS |
| WD | 10 mm |
| Instrument Feature Cutoff | 4 px (~0.25 μm) |
| Deconvolution | Au, C, Pd, O |
| Element List | Si, Al, Ca, Mg, Ba, Na, K, Ti, Cr, Mn, Fe, Co, Ni, Cu, Zn, Mo, Sn, Sb, Nd, N, F, Cl, S, P |
| Quant Standardizations | Factory Quant Standardizations |

Table 4. Strongly correlated particle classes (Kendall's Tau, α = 0.01).

|  |  | p-value | $\tau$ |
|---|---|---|---|
| Si.Al.Mg.Fe | Si.Al.K.Fe | 0.0081 | 3.5 |
| Si.Al.Mg.K.Fe | Si.Al.K | 0.0081 | 6.3 |
| Si.Al.Na.K | Si.Al.K | 2.00E-04 | 3.5 |
| Si.Al.Ca.Fe | Si.Al.Fe | 0.0081 | 3.5 |
| Si.Al.Na.Fe | Si.Al.Fe | 0.0081 | 4.9 |
| Si.Al.Ti.Fe | Si.Al.Fe | 0.0081 | -4.1 |
| Si.K.P | Si.K | 0.0012 | 3.5 |
| Si.Al.Ca.Na | Si.Al.Mg.Fe | 0.0081 | 3.5 |
| Si.Al.Ca.Mg.Fe | Si.Al.Mg.Fe | 0.0081 | -3.5 |
| Si.Al.Ca.Na | K | 0.0081 | 3.5 |
| Si.Al.Ca.Na | Si.Al.Na | 0.0081 | -4.1 |
| Si.Al.Na.Fe | Si.Al | 0.0081 | 3.5 |
| Si.Al.Na.K | Si.Al.Mg.K.Fe | 0.0081 | 3.5 |
| Si.Al.Ca.Na.Fe | Si.Al.Ca.Mg.Fe | 0.0081 | -3.5 |
| Si.Al.Ti.Fe | Si.Al.Ca.Mg.Fe | 0.0081 | 3.5 |

Table 5. Strongly correlated particle subclasses ( Kendall's Tau, α = 0.01).

|  |  | p-value | τ |
|---|---|---|---|
| Si.Al.Mg.Fe_2 | K_1 | 0.0081 | -3.5 |
| Si.K_0 | K_1 | 0.0081 | 3.5 |
| Si.Al.Ca.Na_1 | K_1 | 8.10E-03 | -3.5 |
| Si.Al.Ca.Na_1 | Si.Al.Mg.Fe_2 | 0.0035 | 4.1 |
| Si.Al.Ca.Mg.Fe_1 | Si.Al.Mg.Fe_2 | 0.0081 | 3.5 |
| Si.Al.Ca.Na_1 | Si.Al.Na_1 | 0.0035 | 4.1 |
| Si.Al_1 | Si.Al.Na_1 | 0.0081 | 3.5 |
| Si.Al.Fe_4 | Si.K_0 | 0.0081 | -3.5 |
| Si.K.P_0 | Si.K_0 | 0.0081 | 3.5 |
| Si.Al.K.Fe_2 | Si.Al.K.Fe_3 | 0.0081 | 4.1 |
| Si.Al.Na.K_1 | Si.Al.K.Fe_3 | 0.0012 | 4.9 |
| Si.Al.K_1 | Si.Al.K.Fe_3 | 0.0012 | 4.9 |
| Si.Al.Na.Fe_1 | Si.Al.Fe_2 | 0.0081 | 3.5 |
| Si.Al.Ca.Mg.Fe_1 | Si.Al.Ca.Na_1 | 0.0081 | 3.5 |
| Si.Al_1 | Si.Al.K.Fe_2 | 0.0081 | 3.5 |
| Si.Al.Ca.Fe_1 | Si.Al.Fe_1 | 0.0012 | 3.5 |
| Si.Al.Na.Fe_1 | Si.Al.Ca.Fe_1 | 0.0012 | 9.2 |
| Si.Al.Mg.Fe_1 | Si.Al.Ca.Fe_1 | 0.0035 | 4.9 |
| Si.Al.Ca.Mg.Ti.Fe_0 | Si.Al.Ca.Fe_1 | 0.0081 | 3.5 |
| Si.Al.Ca.Na.Fe_1 | Si.Al.Ca.Mg.Fe_1 | 0.0035 | 4.9 |
| Si.Al_2 | Si.Al_3 | 0.0081 | 4.1 |

Table 5. (cont.)

|  |  | p-value | $\tau$ |
|---|---|---|---|
| K.S_2 | Si.Al_1 | 0.0081 | 4.1 |
| Si.Al.K_1 | Si.Al.K.Fe_1 | 0.0035 | 4.1 |
| Si.Al.Ca.Fe_3 | Si.Al.Fe_3 | 0.0081 | 4.1 |
| Si.Al.Fe_0 | Si.Al.Na.Fe_1 | 0.0035 | 3.5 |
| Si.Al.Mg.Fe_1 | Si.Al.Na.Fe_1 | 0 | 4.1 |
| Si.Al.Ti.Fe_4 | Si.Al.Na.Fe_1 | 0.0081 | 3.5 |
| Si.Al.K_3 | Si.Al.Ca_2 | 0.0035 | 3.5 |
| Si.Al.Ca.Na.Fe_1 | Si.Al.Fe_4 | 0.0035 | 6.3 |
| Si.Al.Mg.Fe.S_0 | Si.Al.Fe_4 | 0.0081 | 4.1 |
| Si.Al.K_1 | Si.Al.Na.K_1 | 0.0035 | 3.5 |
| Si.Al.Mg.Fe.S_0 | Si.K.P_0 | 0.0081 | 4.1 |
| K.S_2 | Si.Al.Na_0 | 0.0081 | 3.5 |
| Si.Ca.K_1 | Si.Al.Mg.Fe_0 | 0.0081 | 3.5 |
| Si.Al.Mg.Fe_1 | Si.Al.Fe_0 | 0.0012 | 3.5 |
| Si.Al.Ca.K.Ti.Fe_0 | Si.Ca.K.Fe_0 | 0.0035 | 4.1 |

Table 6. Source class particle density (percent observed).

| | n | AVG | DV1 | DV2 | DV3 | DV4 | DV5 | DV6 | U1 | U2 | U3 | PD |
|---|---|---|---|---|---|---|---|---|---|---|---|---|
| soil | 5321 | 28.6 | 34.8 | 21.9 | 29.5 | 24.7 | 44.8 | 33.1 | 24 | 18.7 | 19.7 | 23.3 |
| unknown | 4829 | 26 | 22.4 | 37.7 | 22.9 | 25 | 15 | 25.8 | 24.5 | 39.8 | 18.5 | 38.1 |
| mineral | 3738 | 20.1 | 26 | 24.7 | 18.4 | 22 | 19.8 | 19.1 | 16.5 | 19.8 | 16.7 | 17.8 |
| quartz | 1857 | 10 | 6.8 | 6.8 | 14.5 | 8.8 | 10.5 | 13.4 | 13 | 10.8 | 8.7 | 7 |
| vehicle/ industrial | 1419 | 7.6 | 2 | 2.2 | 3.3 | 12.5 | 3 | 3.8 | 13.2 | 3.2 | 25.2 | 9.5 |
| marl | 472 | 2.5 | 3.2 | 2.2 | 3.8 | 1.7 | 2.6 | 2.1 | 3.4 | 2.5 | 2.1 | 1.7 |
| brake | 459 | 2.5 | 2.2 | 1.1 | 2.8 | 1.5 | 3.3 | 2 | 4.2 | 1.3 | 4.5 | 1.3 |
| tire | 192 | 1 | 0.9 | 0.8 | 0.6 | 1.3 | 0.8 | 0.6 | 0.9 | 0.3 | 3.9 | 0.1 |
| biogenic | 190 | 1 | 1.2 | 2.2 | 2.7 | 1.8 | 0.1 | 0.1 | 0.1 | 2.4 | 0.4 | 0.4 |
| calcite | 104 | 0.6 | 0.6 | 0.4 | 1.5 | 0.7 | 0.2 | 0 | 0.3 | 1.2 | 0.5 | 0.7 |
| n | 18581 | 6935 | 6709 | 6718 | 6836 | 5651 | 9487 | 8033 | 5720 | 4428 | 9056 | 7110 |

Table 7. All subclass PCA ordination for the 12 strongest positive and negative scores. Source classes are displayed below each subclass in parenthesis.

| | PC1 | | PC2 | | PC3 | | PC4 |
|---|---|---|---|---|---|---|---|
| Si.Al.Na.K.Fe_0 | | Si.Fe.S.P_0 | | Si.Al.Ti.Fe.P_0 | | Ca.K.Cl_3 | |
| (unknown) | 0.0721 | (unknown) | 0.1013 | (unknown) | 0.0001 | (mineral) | 0.0000 |
| Si.Al.Fe_3 | | Si.Al.Ca.Na.Fe_0 | | Si.Al.Ca.K.Fe_0 | | K.S.P_2 | |
| (brake) | 0.0718 | (unknown) | 0.1013 | (unknown) | 0.0723 | (mineral) | 0.0814 |
| Si.Al.K.Fe_4 | | Si.Al.Ca.Mg.K.S.P_0 | | N_1 | | Si.S.P_0 | |
| (soil) | 0.0701 | (unknown) | 0.1013 | (unknown) | 0.0719 | (unknown) | 0.0788 |
| Si.K.Fe_1 | | Si.Al.Ca.K.Cl.S_0 | | Si.Al.Na_0 | | Ti.Fe_1 | |
| (unknown) | 0.0687 | (unknown) | 0.1013 | (unknown) | 0.0658 | (vehicle_industrial) | 0.0751 |
| Si.Al.Ca.Ti.Fe_0 | | Si.Al.Mg.K.Fe.Cl_0 | | Si.Al_5 | | Si.Al.Ca.Fe_0 | |
| (unknown) | 0.0683 | (unknown) | 0.1013 | (brake) | 0.0634 | (unknown) | 0.0737 |
| Si.Al.Na.Fe_0 | | Ca.Mg.Fe.S.P_0 | | Si.Al_3 | | Ca.P_3 | |
| (unknown) | 0.0679 | (unknown) | 0.1013 | (soil) | 0.0597 | (mineral) | 0.0712 |
| Mg.Fe_0 | | Ca.P_2 | | Si.Ca.Mg.Ti.Fe_0 | | Si.Ca.Mg.K.Ti.Fe_0 | |
| (unknown) | 0.0671 | (mineral) | 0.1013 | (unknown) | 0.0597 | (unknown) | 0.0712 |
| Si.Fe_2 | | Si.Ca.Nd.P_0 | | Si.Al.Ti.Fe_1 | | Si.Al.K.Co_0 | |
| (vehicle_industrial) | 0.0643 | (unknown) | 0.1013 | (mineral) | 0.0584 | (unknown) | 0.0712 |
| Si.Fe_3 | | Si.Al.Ca.Mg.K.Fe.Cl_0 | | Si.Al_4 | | Si.Ca.Mg.Fe.P_0 | |
| (vehicle_industrial) | 0.0641 | (unknown) | 0.1013 | (soil) | 0.0582 | (unknown) | 0.0712 |
| Si.Ca.Ti.Fe_2 | | Si.Al.Ca.Mg.K_1 | | Si.Mg.Fe_0 | | Cr_1 | |
| (unknown) | 0.0615 | (mineral) | 0.1013 | (unknown) | 0.0582 | (vehicle_industrial) | 0.0712 |
| Fe_1 | | Si.Al.Ca.Na.P_0 | | Si.Al.K.Ti.Fe_1 | | Ca.K.Fe.S_0 | |
| (vehicle_industrial) | 0.0606 | (unknown) | 0.1013 | (unknown) | 0.0554 | (unknown) | 0.0712 |
| Si.Ca.Fe_3 | | Ca.F.P_0 | | Si.Mg.Ti.Fe_0 | | Si.Ti.S_0 | |
| (mineral) | 0.0598 | (unknown) | 0.1013 | (unknown) | 0.0530 | (unknown) | 0.0712 |

Table 7. (cont.)

| | PC1 | | PC2 | | PC3 | | PC4 |
|---|---|---|---|---|---|---|---|
| Si.Ca_1 | | Si.Na.K_0 | | Si.Al.Ca.Na.Fe_0 | | Si.Sb_0 | |
| (marl) | -0.0061 | (unknown) | -0.0016 | (unknown) | -0.0045 | (unknown) | -0.0003 |
| Si.Al.Ca.Na_0 | | Si.Al.Ca.Na.K.Fe_0 | | Ca.P_2 | | Si.Na.K.Fe_0 | |
| (unknown) | -0.0055 | (unknown) | -0.0013 | (mineral) | -0.0045 | (unknown) | -0.0003 |
| Si.Al.K_0 | | Si.S_0 | | Si.K.Fe.Cl.S_0 | | Si.Al.N_0 | |
| (unknown) | -0.0045 | (unknown) | -0.0013 | (unknown) | -0.0045 | (unknown) | -0.0003 |
| Si.Al.Mg.K.Fe_2 | | Si.Al.Ca.Mg.K.Fe_0 | | Si.Mg.Ti.Fe.S_0 | | Sn_1 | |
| (mineral) | -0.0037 | (unknown) | -0.0012 | (unknown) | -0.0045 | (unknown) | -0.0003 |
| Si.Al.Ca.K.Fe_0 | | Si.Fe_1 | | Si.Al.Ca.Na.K_2 | | Si.Ti.Fe.Cu.Sn.S_0 | |
| (unknown) | -0.0029 | (mineral) | -0.0007 | (unknown) | -0.0035 | (unknown) | -0.0003 |
| Si.Al.Ca.Fe.S_2 | | Mn.Fe_1 | | Si.Al.Ca.Na_2 | | Cr.Fe.Ni_1 | |
| (mineral) | -0.0027 | (vehicle_industrial) | -0.0006 | (mineral) | -0.0034 | (vehicle_industrial) | -0.0003 |
| Si.Al.Ca.Ti_1 | | Si.Ca.Mg.K.Fe.P_0 | | Ti.Fe_1 | | Si.Al.Ca_0 | |
| (mineral) | -0.0019 | (unknown) | -0.0006 | (vehicle_industrial) | -0.0026 | (unknown) | -0.0003 |
| Si.Ca.Mg.Fe_1 | | Si.Al.Mg.Na.Fe.S_0 | | Ca.K_1 | | Ca.Ti.Fe.Zn.Sn_0 | |
| (unknown) | -0.0016 | (unknown) | -0.0006 | (biogenic) | -0.0024 | (unknown) | -0.0003 |
| Si.Al.Na.S_0 | | Cl_1 | | Si.N_0 | | Si.Al.Mg.K.Mn.Fe_0 | |
| (unknown) | -0.0015 | (mineral) | -0.0006 | (unknown) | -0.0021 | (unknown) | -0.0003 |
| Si.Ca.Mg.Fe_0 | | Si.Ca.Mg_1 | | Si.Al.Ca.S.P_0 | | Si.Al.Fe.Zn.S_0 | |
| (unknown) | -0.0010 | (mineral) | -0.0006 | (unknown) | -0.0020 | (unknown) | -0.0003 |
| Si.Al.Ca.Na.S_1 | | Si.Al.Ca.Na.K_2 | | Si.Al.Ca.Mg.K_0 | | Si.Al.Ti.Fe.Zn.Sn.S_0 | |
| (mineral) | -0.0008 | (unknown) | -0.0004 | (unknown) | -0.0008 | (unknown) | -0.0003 |
| Si.Al.Ca.Na.Ti.Fe_0 | | Ca_1 | | Si.Al.K.S.P_0 | | Ti.Fe.Zn_0 | |
| (unknown) | -0.0004 | (calcite) | -0.0004 | (unknown) | -0.0002 | (unknown) | -0.0003 |

Table 8. Common subclass PCA ordination for the 12 strongest positive and negative scores. Subclasses that appear on less than 80% of locations were not included.

| | PC1 | | PC2 | | PC3 |
|---|---|---|---|---|---|
| Si.Al.Fe_2 (soil) | 0.2266 | Si.Al.Mg.K.Fe_0 (unknown) | 0.2388 | Si.Al.Ca.K_2 (mineral) | 0.2899 |
| Si.Al.Fe_1 (soil) | 0.2146 | Si.Al.Ca.K.Fe_1 (soil) | 0.2202 | Si.Al.Ca.Mg.K.Fe_1 (mineral) | 0.2815 |
| Si.Al.Ca.Mg.Fe_0 (unknown) | 0.2044 | Si.Al.Ca.K.Fe_5 (mineral) | 0.2041 | Si.Al.K.Fe.S_1 (mineral) | 0.2593 |
| Si.Al.Mg.Fe_2 (soil) | 0.1974 | Si.Al.K.Fe_3 (soil) | 0.1989 | Si.Al.Ca.Na.K_1 (mineral) | 0.2346 |
| Si.Al.Ca_2 (marl) | 0.1941 | Si.Mg.K.Fe_0 (unknown) | 0.1906 | Si.Al.Na.K.Fe_1 (mineral) | 0.2041 |
| Si.Fe_1 (mineral) | 0.1906 | Si.Al.K_2 (soil) | 0.1795 | Si.Al.Ca_1 (marl) | 0.1997 |
| Si.Al.Ca.K_1 (mineral) | 0.1881 | Si.Al.K_0 (unknown) | 0.1721 | Si.Al.Ca.K.Fe_2 (soil) | 0.1924 |
| Si.Al.Fe_3 (brake) | 0.1876 | Si.Al.K.Fe_1 (soil) | 0.1676 | Si.Ca.Mg.Fe_1 (unknown) | 0.1891 |
| Si.Ca.Ti_1 (mineral) | 0.1871 | Si.Al.K_4 (mineral) | 0.1654 | Si.Ca.K_3 (mineral) | 0.1870 |
| Si.Al.Na_1 (soil) | 0.1830 | Si.Al.Ca.K.Fe_2 (soil) | 0.1639 | Si.Al.Fe.S_1 (tire) | 0.1820 |
| Si.Mg.Fe_2 (mineral) | 0.1771 | Si.Al.K.P_0 (unknown) | 0.1618 | Si.Ca.K.Fe_0 (unknown) | 0.1688 |
| Si.Al.K_3 (unknown) | 0.1761 | Si.Al.Ca.Ti.Fe_1 (vehicle_industrial) | 0.1458 | Si.Al.Na.K_0 (unknown) | 0.1682 |

Table 8. (cont.)

| | PC1 | | PC2 | | PC3 |
|---|---|---|---|---|---|
| Si.K_1 (mineral) | -0.0913 | Si.K.Fe_1 (unknown) | -0.0893 | Si.Mg.K.Fe_0 (unknown) | -0.0399 |
| Si.Al.Ca.K.Fe_0 (unknown) | -0.0710 | Si.Al.K.Fe.S_1 (mineral) | -0.0847 | Si.Al.Mg.Fe_2 (soil) | -0.0297 |
| Si.Al.Ca_3 (marl) | -0.0484 | Si.Al.K.Ti.Fe_0 (unknown) | -0.0765 | Si.Al.K_4 (mineral) | -0.0227 |
| Si.Al.Ca.K.Fe_5 (mineral) | -0.0418 | Si.Al.Na.K.Fe_1 (mineral) | -0.0721 | Ca_1 (calcite) | -0.0212 |
| Si.Al.Ca.Na_2 (mineral) | -0.0402 | Si.Al.K.Fe_0 (unknown) | -0.0472 | Si.Al.Fe_1 (soil) | -0.0162 |
| Si.Al.K.Fe.S_1 (mineral) | -0.0396 | Si.K.Ti.Fe_0 (unknown) | -0.0398 | K.Fe_0 (unknown) | -0.0119 |
| K.Fe_0 (unknown) | -0.0345 | K.Fe_0 (unknown) | -0.0370 | Si.Al.K.Fe_4 (soil) | -0.0104 |
| Si.Al.Ca.K.Fe_2 (soil) | -0.0338 | Si.Ca.Mg.Fe_1 (unknown) | -0.0357 | Si.Al.K.Fe_0 (unknown) | -0.0101 |
| Si.Al.Ca.K_2 (mineral) | -0.0298 | Ca_1 (calcite) | -0.0313 | Si.Mg.Fe_2 (mineral) | -0.0085 |
| Si.Al.Ca.Na.K_1 (mineral) | -0.0295 | Si_1 (quartz) | -0.0188 | Si.Ca.Ti_1 (mineral) | -0.0050 |
| Si.Al.Ca.K.Fe_1 (soil) | -0.0190 | Si.Ca_3 (marl) | -0.0163 | Si.Al.K_2 (soil) | -0.0046 |
| Si.Al.K.P_0 (unknown) | -0.0113 | Si.Al.Ca.K.Fe_0 (unknown) | -0.0056 | Si.Al.Fe_2 (soil) | -0.0022 |
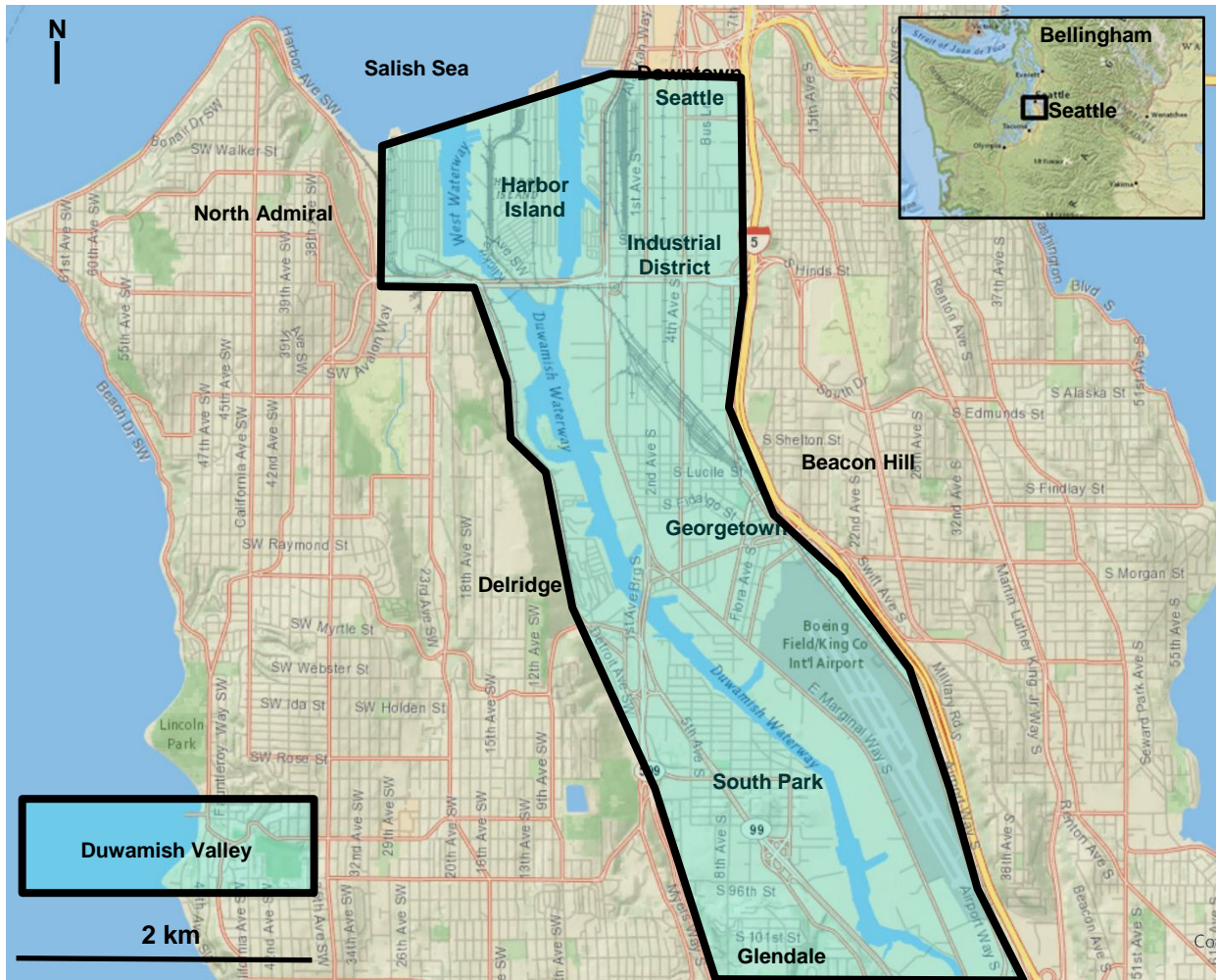
Figure 1. The Duwamish Valley (outlined) and surrounding areas. Downtown Seattle, Harbor Island, North Admiral, Industrial District, Beacon Hill, Georgetown, Delridge, and South Park are regions within Seattle. Glendale is a region of Burien, which is immediately south of Seattle and considered a part of the Seattle area.
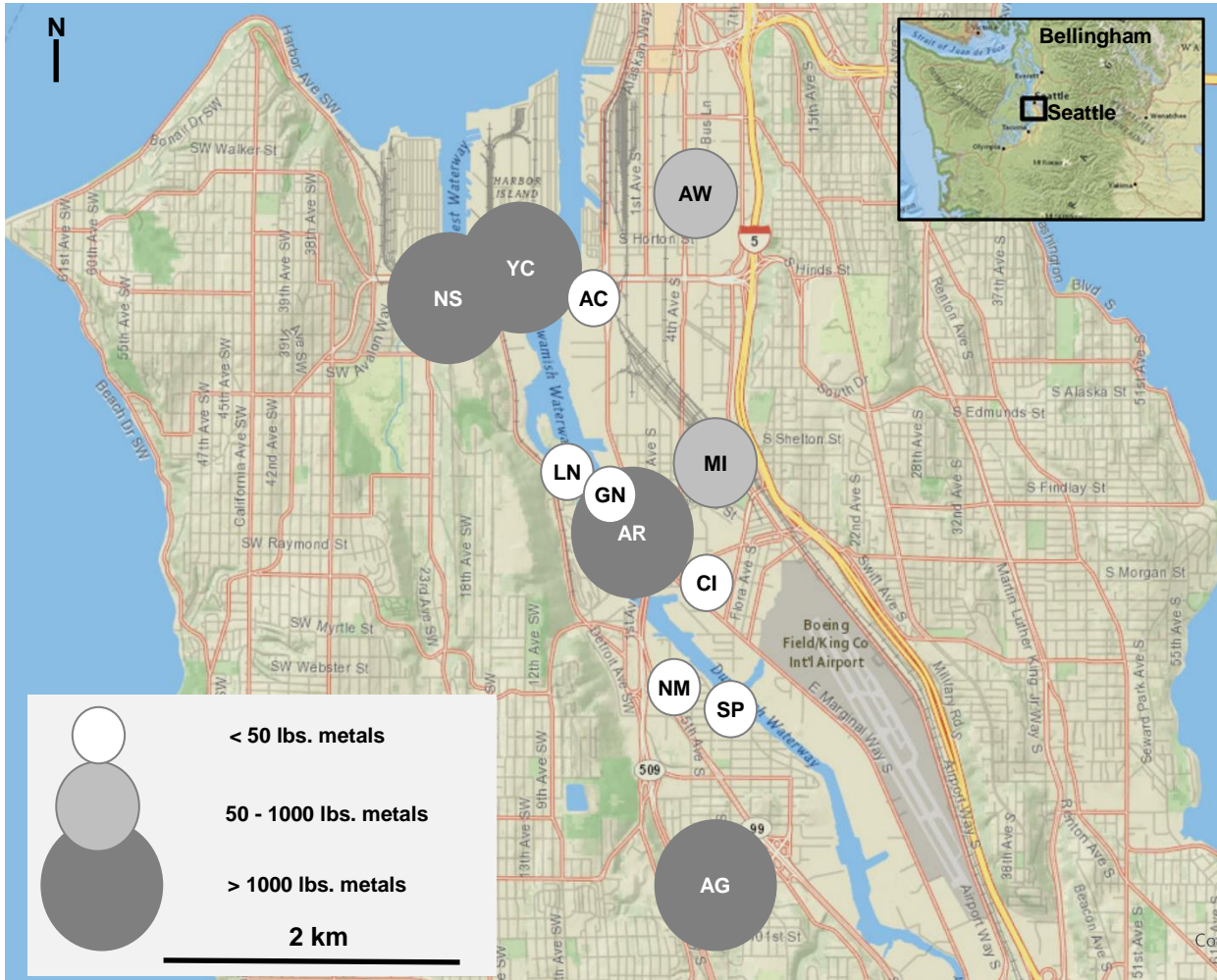
Figure 2. Distribution of reported air emissions of metals in the study region, colored by weight of metals released into the air in 2017 (US EPA 2018b; USGS, 2018; Appendix A). Facility codes and emission details are reported in Table 1.

Figure 3. Distribution of lichen bag deployment locations (USGS, 2018). The location of the larger emitters from Figure 1 are displayed as grey circles. Location codes are defined in Table 2.

Figure 4. Lichen bag deployment setup.
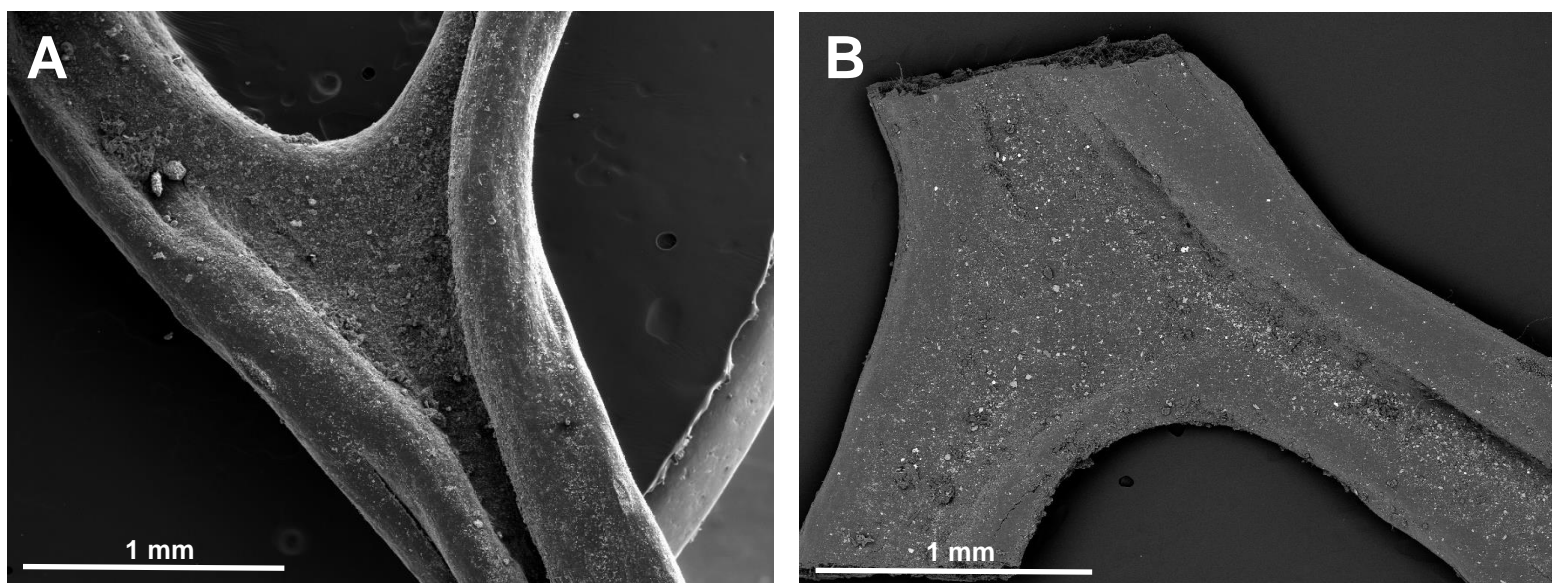
Figure 5. Lichen sample region under primary (A) and secondary (B) electron microscope at 50x magnification.
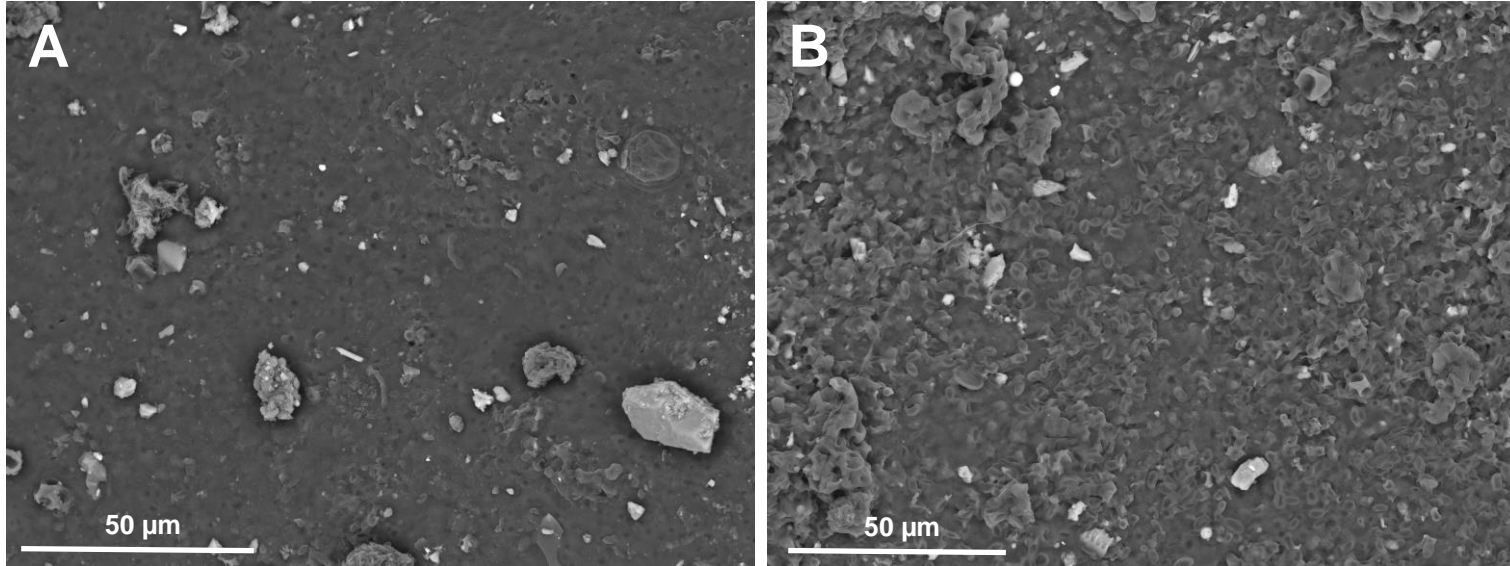
Figure 6. Ideal lichen substrate for PM analysis including sooth (A) and rough (B).
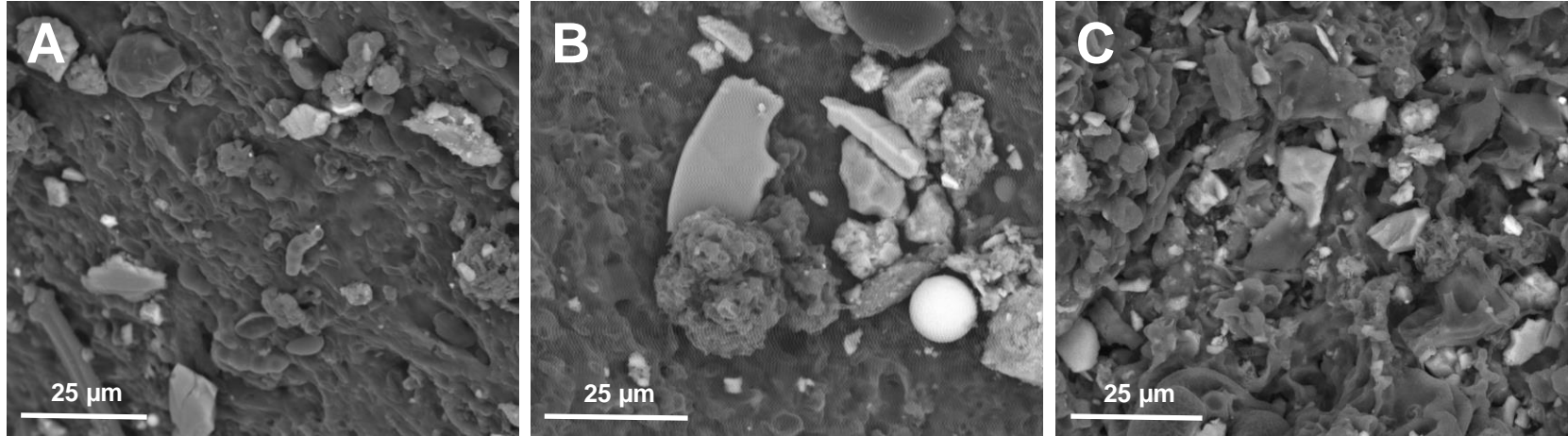
Figure 7. Common issues with lichen substrate, including poor focus from curved surface (A), overlapping PM (B), and irregular substrate obscuring PM (C).
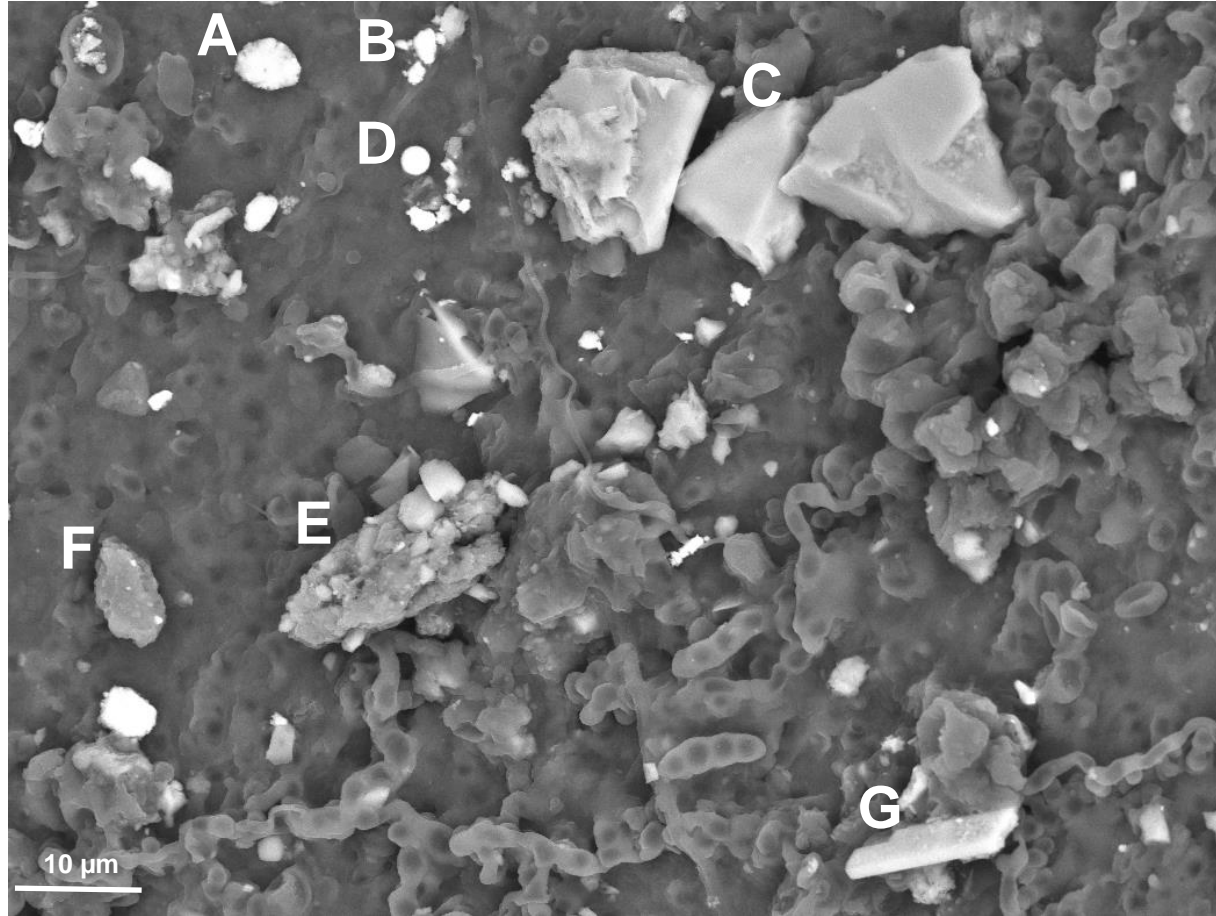
Figure 8. Common particle morphologies including irregular (A), clustered (B), angular (C), spheroid (D), polymineralic (E), rough (F), and oblong (G).
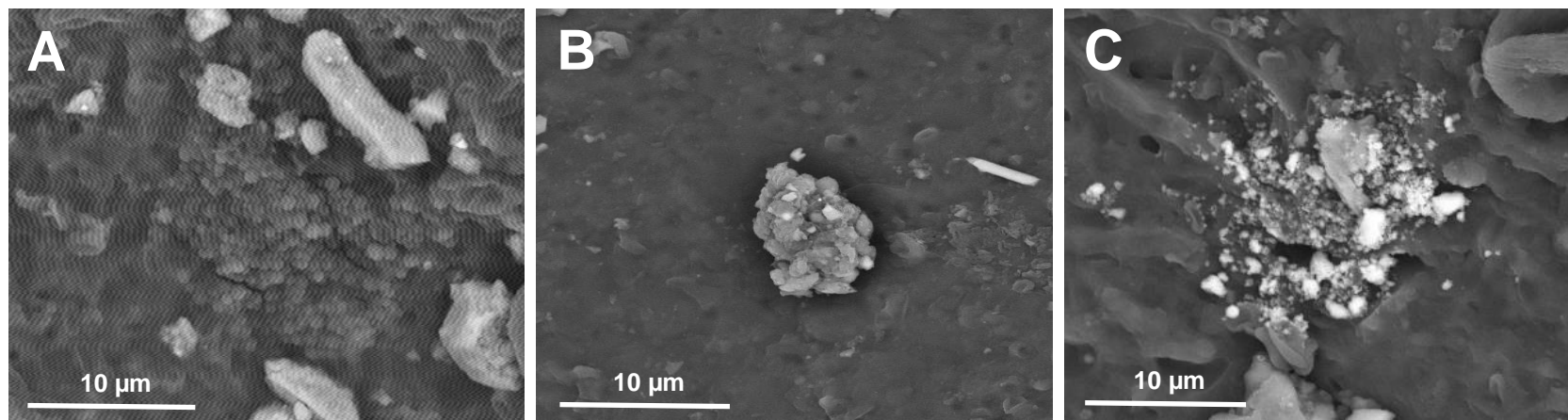
Figure 9. Manually identified particles including carbonaceous (A), polymineralic (B), and clustered debris (C).
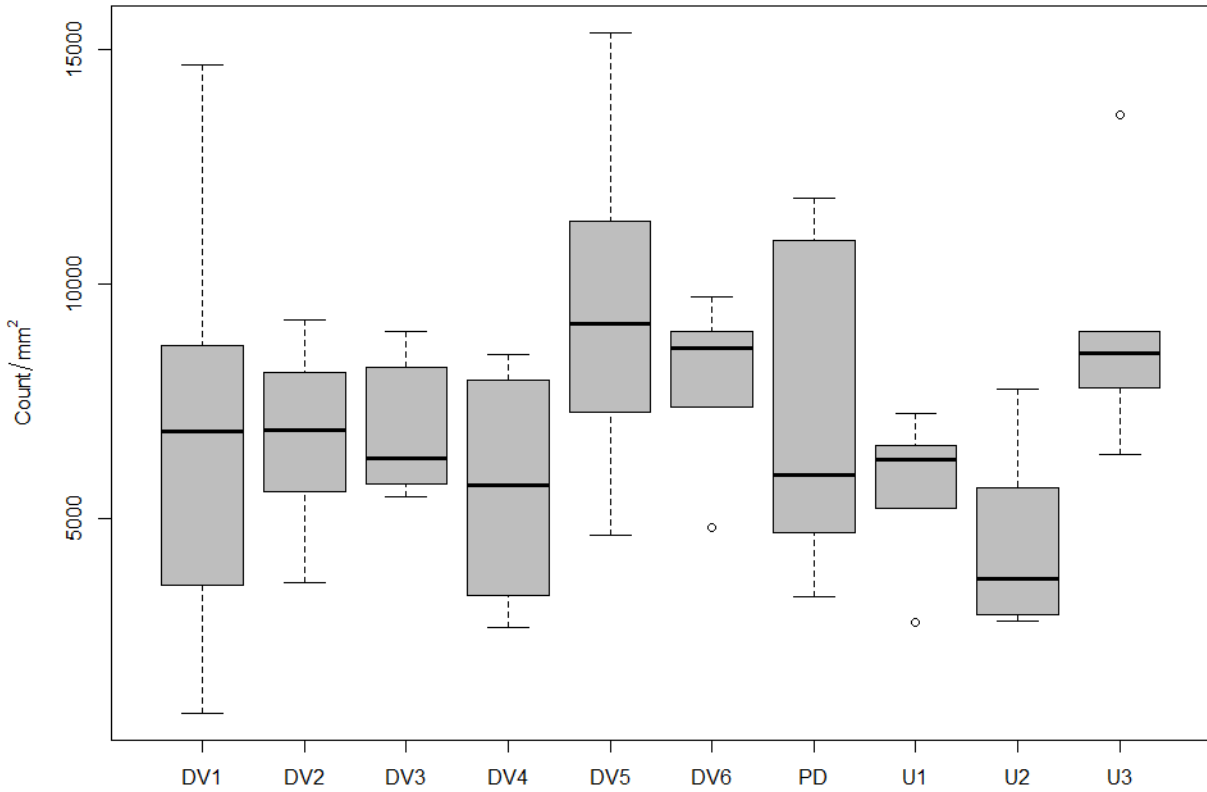
Figure 10. Particle frequency in each location. Median, quartiles, minimum, maximum, and outliers are shown. Location codes are defined in Table 2.
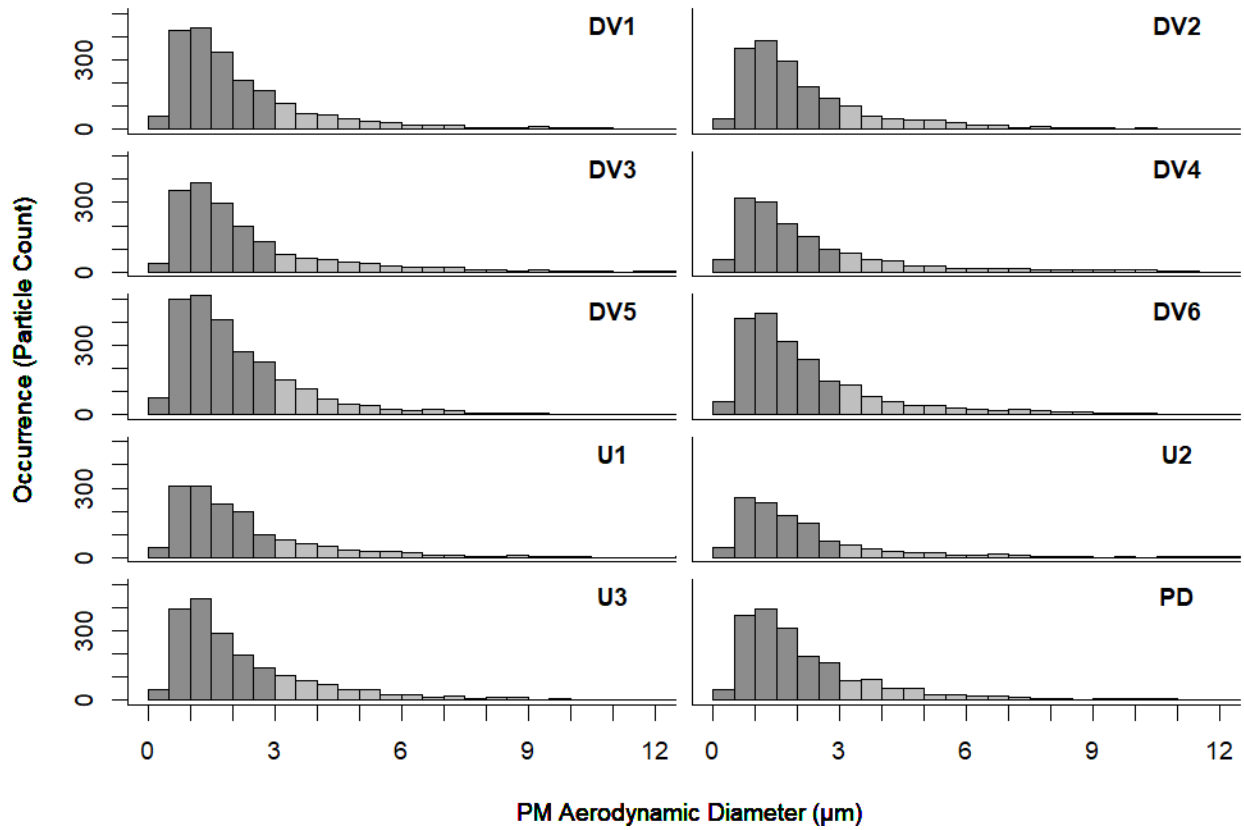
Figure 11. Particle size distribution colored by $PM_{2.5}$ and $PM_{10}$ cutoffs. Location codes are defined in Table 2.
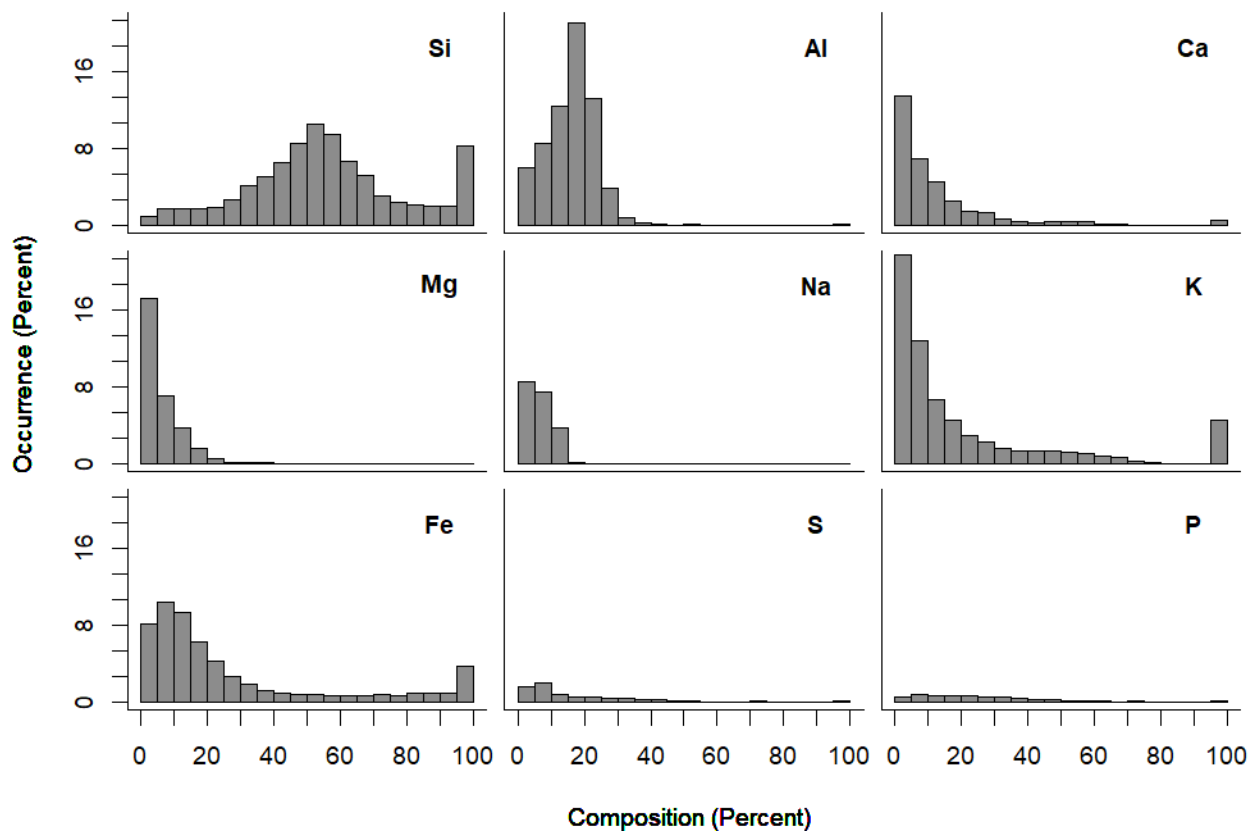
Figure 12. Particle composition distribution for the nine most common elements across all particles. Frequencies with less than 5% composition were not included.
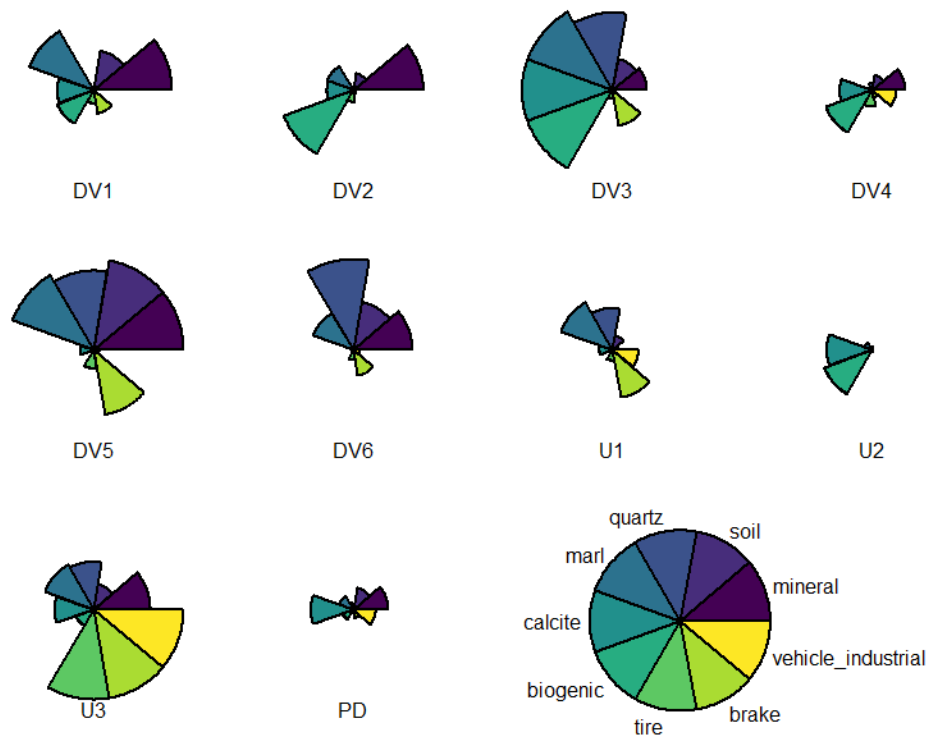
Figure 13. Source class frequency at each location. Area represents relative frequency of each source class compared to the maximum count observed in a single location.
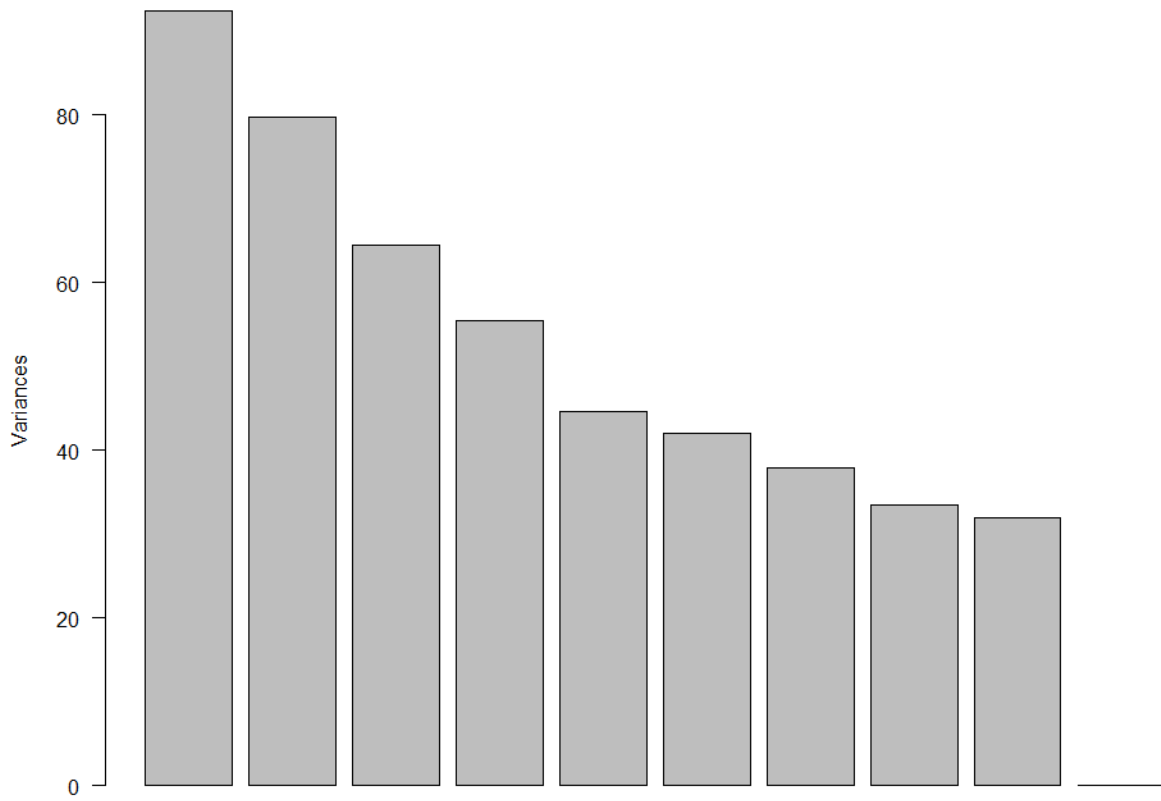
Figure 14. PCA variance for all subclass frequencies.
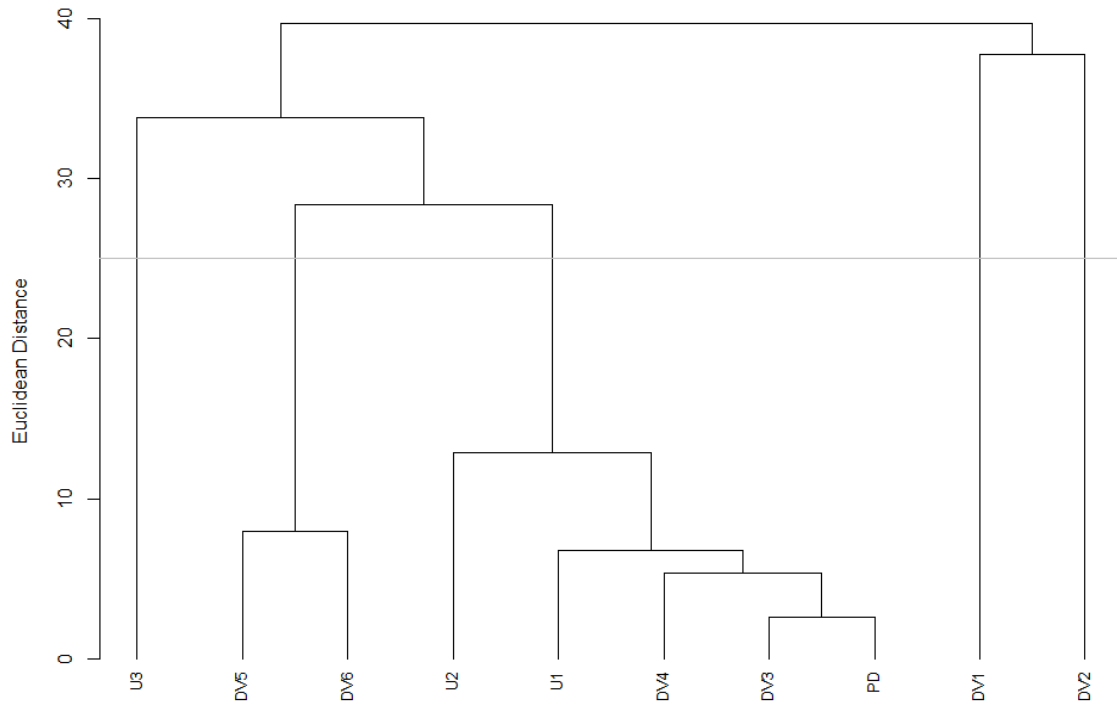
Figure 15. Hierarchical clustering on PCA for all subclass frequencies using Ward's method. Two groups and three outliers are formed, consisting of DV5 and DV6 together, U1, U2, DV3, DV4, and PD together, and U3, DV1, and DV2 separated from the rest.
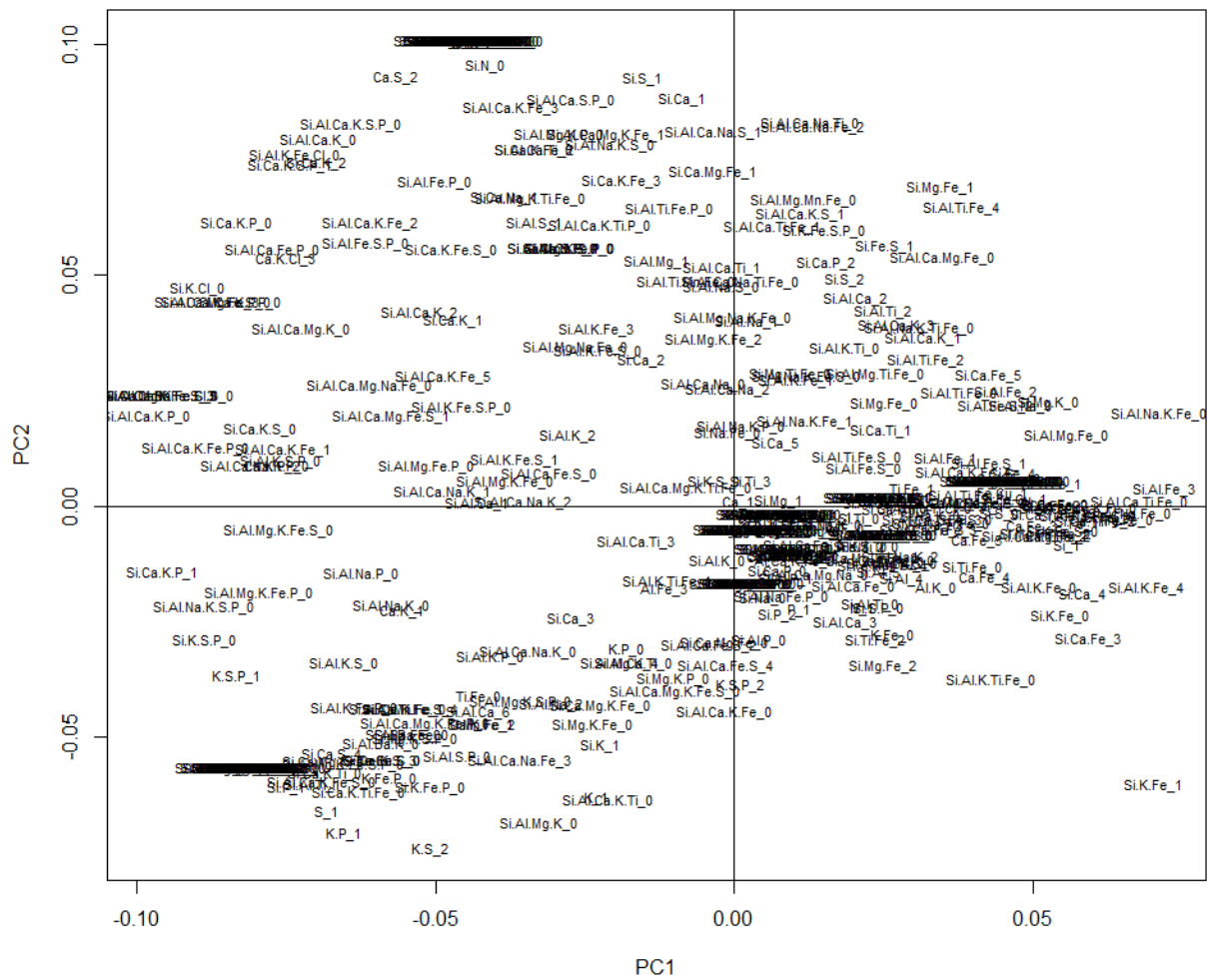
Figure 16. PC1 and PC2 scores for all subclass frequencies.
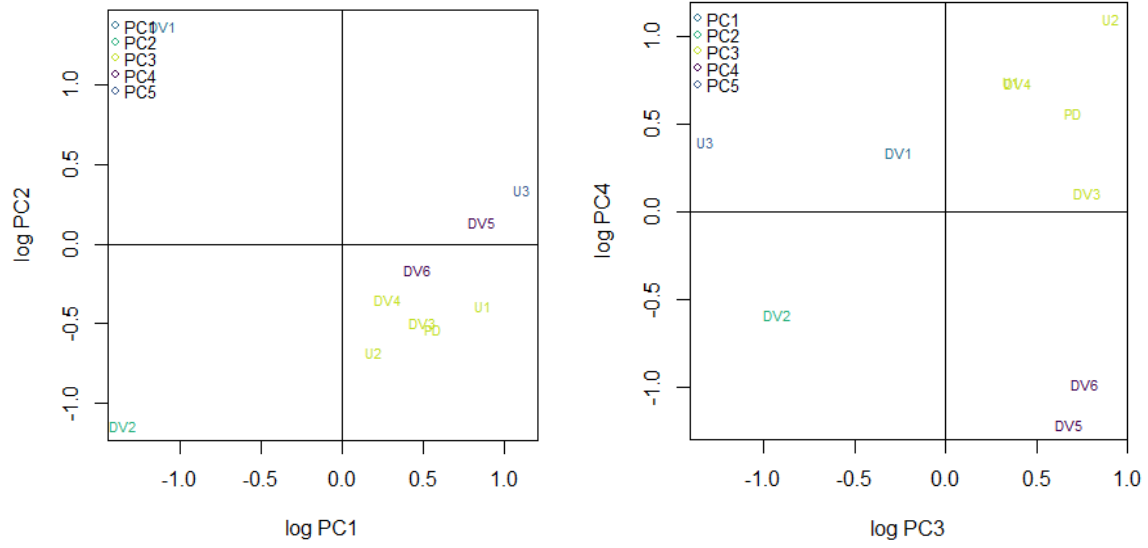
Figure 17. Location ordination on PC1 through PC4 using all subclass frequencies.
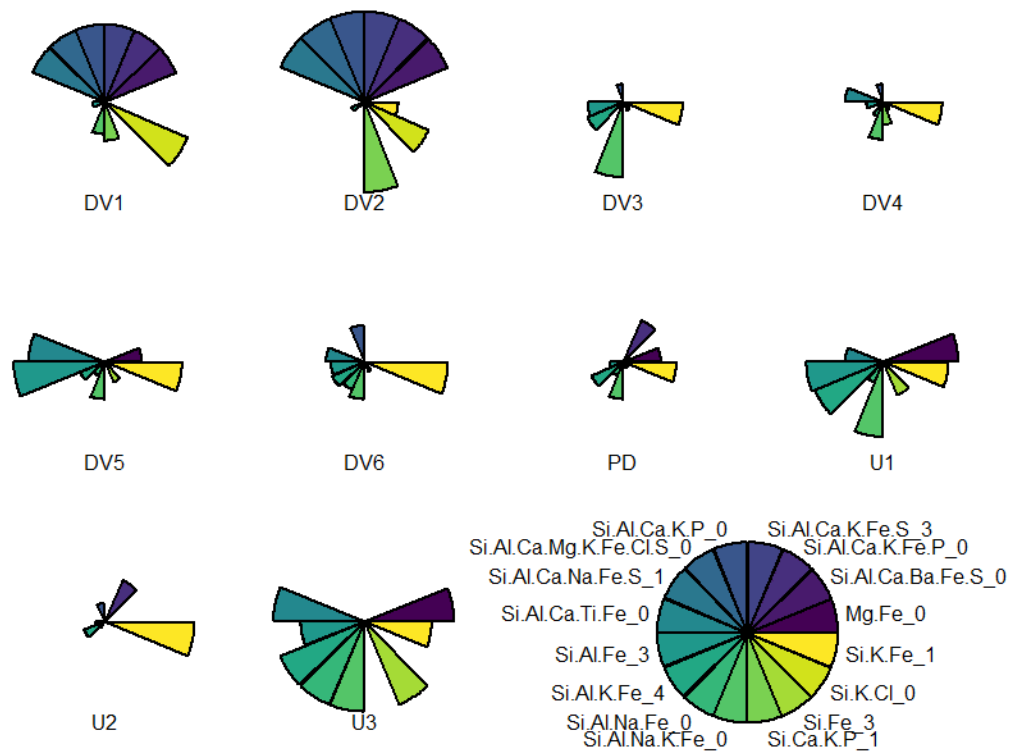
Figure 18. Star pots of subclass frequency at each location using the eight highest and lowest scoring particle subclasses from PC1 for all subclass frequencies. Area represents relative frequency of each source class compared to the maximum count observed in a single location.
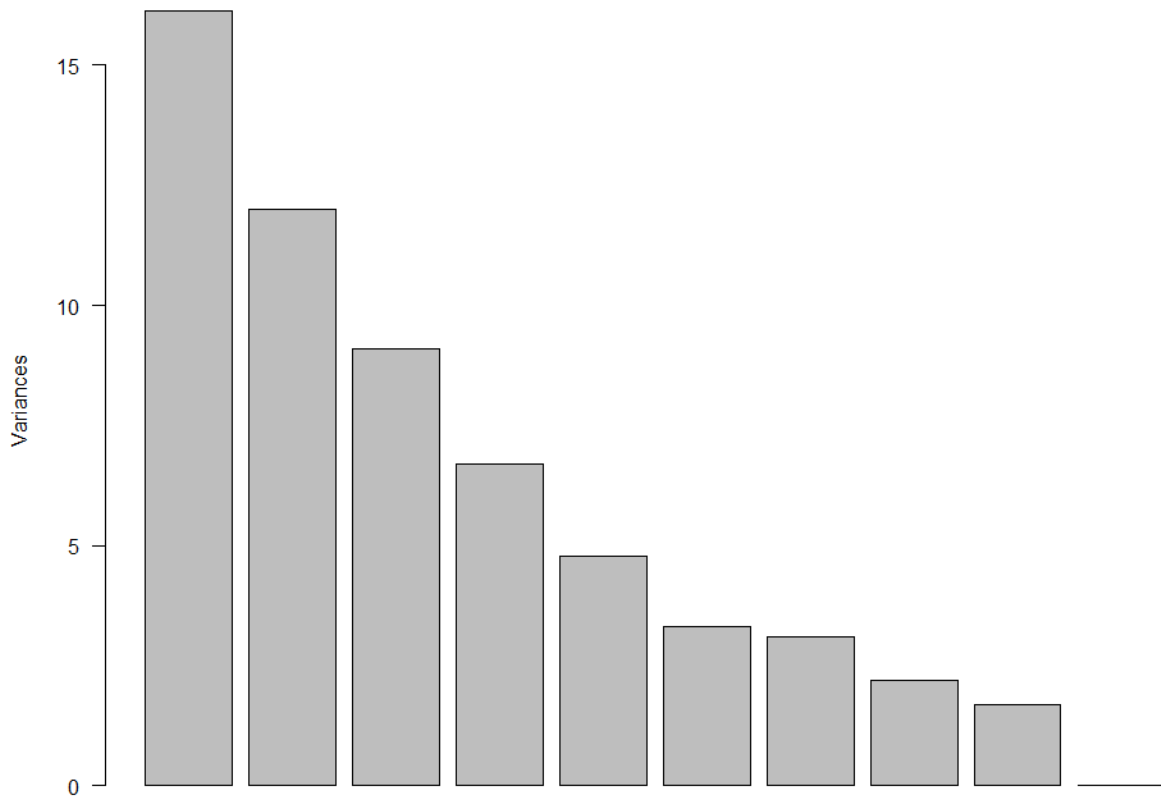
Figure 19. PCA variance for common subclass frequencies. Subclasses that appear on less than 80% of locations were not included.
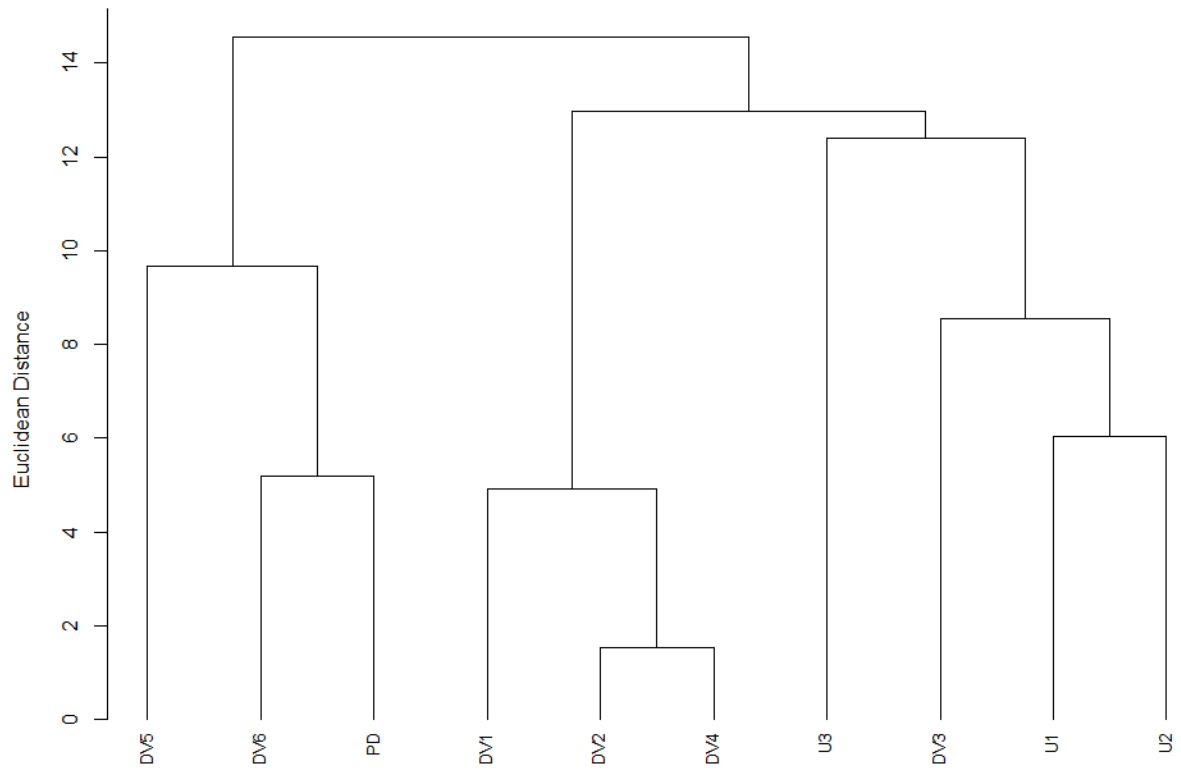
Figure 20. Hierarchical clustering on PCA for common subclass frequencies. Subclasses that appear on less than 80% of locations were not included.

## Appendices

Appendix A. Study region maps.
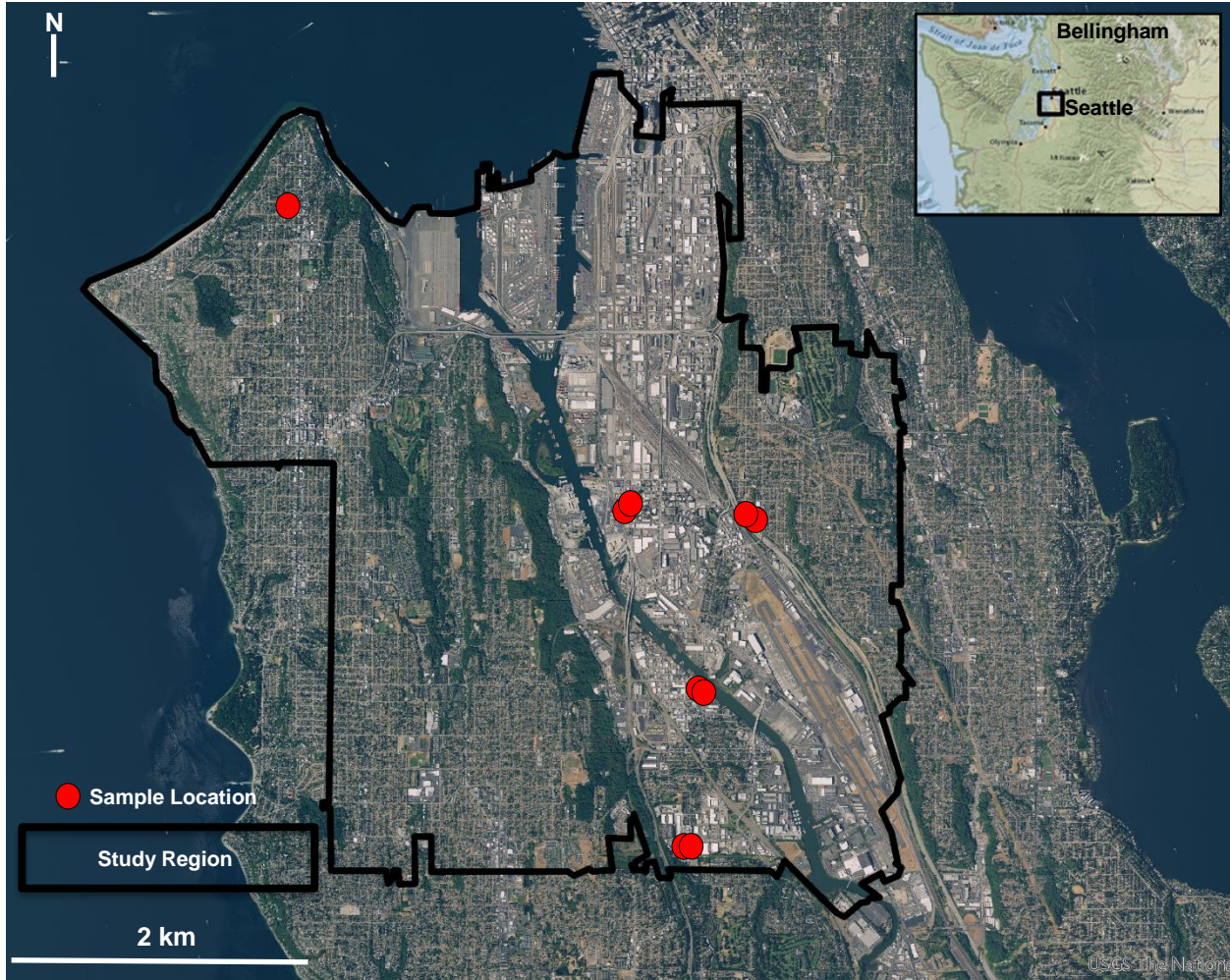


Figure A1. Satellite map of study region (USGS, 2018). The zip codes included in study region emission characterization (98106, 98108, 98116, 98126, and 98134; Table 1) are outlined in black. Sample locations are shown as red circles (Figure 2).
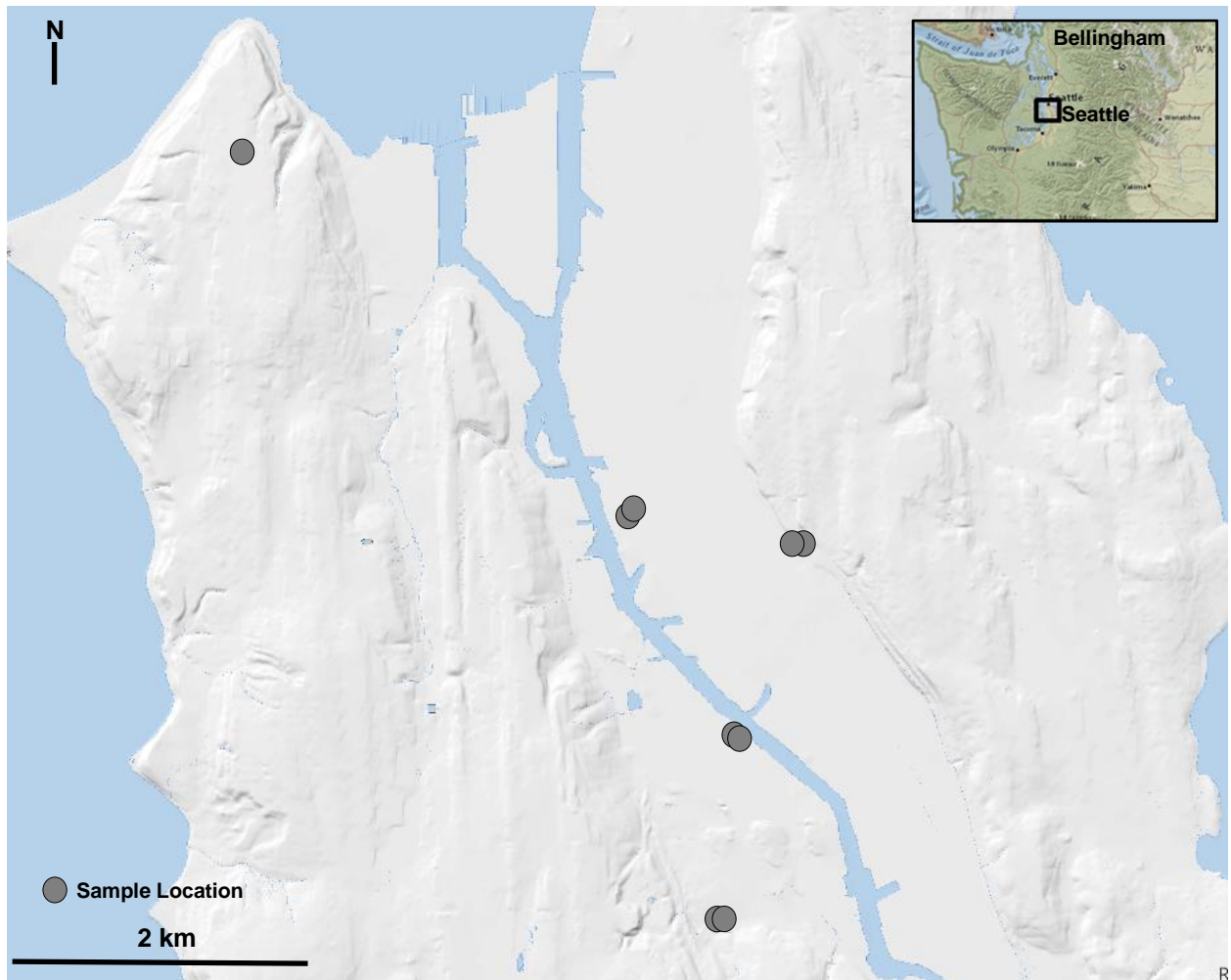
Figure A2. Relief map of study region (USGS, 2018). Sample locations are represented as grey circles (Figure 2).

Appendix B. Subclasses particle density for n >= 10 (particles/mm$^2$).

| | n | Source | AVG | DV1 | DV2 | DV3 | DV4 | DV5 | DV6 | U1 | U2 | U3 | PD |
|---|---|---|---|---|---|---|---|---|---|---|---|---|---|
| Si_1 | 1857 | quartz | 693 | 454 | 459 | 989 | 500 | 1000 | 1079 | 743 | 478 | 784 | 500 |
| K_1 | 854 | unknown | 319 | 35 | 552 | 392 | 246 | 30 | 194 | 194 | 590 | 148 | 825 |
| Fe_1 | 732 | vehicle_industrial | 273 | 22 | 30 | 97 | 537 | 60 | 101 | 355 | 52 | 1241 | 440 |
| Si.Al.Mg.Fe_2 | 722 | soil | 269 | 349 | 198 | 220 | 194 | 649 | 265 | 235 | 153 | 228 | 183 |
| Si.Al.Na_1 | 685 | soil | 256 | 358 | 213 | 299 | 220 | 564 | 314 | 183 | 75 | 202 | 105 |
| Si.K_0 | 515 | unknown | 192 | 83 | 310 | 187 | 190 | 15 | 202 | 168 | 220 | 112 | 440 |
| Si.Al.K_0 | 479 | unknown | 179 | 150 | 164 | 93 | 179 | 187 | 269 | 127 | 157 | 94 | 358 |
| Si.Al.K.Fe_3 | 462 | soil | 172 | 234 | 175 | 153 | 134 | 235 | 261 | 142 | 56 | 108 | 205 |
| Si.K_1 | 462 | mineral | 172 | 115 | 220 | 138 | 216 | 97 | 261 | 142 | 161 | 148 | 231 |
| Si.Al.K_4 | 449 | mineral | 168 | 154 | 172 | 157 | 112 | 258 | 205 | 93 | 105 | 157 | 265 |
| Si.Al.Fe_2 | 417 | soil | 156 | 150 | 75 | 116 | 108 | 381 | 216 | 105 | 93 | 233 | 93 |
| Si.Al.Ca.Na_1 | 411 | mineral | 153 | 192 | 127 | 149 | 127 | 362 | 175 | 142 | 52 | 148 | 52 |
| Si.Al.K.Fe_2 | 377 | soil | 141 | 243 | 97 | 93 | 97 | 265 | 194 | 82 | 71 | 81 | 157 |
| Si.Al.Fe_1 | 372 | soil | 139 | 115 | 101 | 131 | 131 | 325 | 183 | 93 | 52 | 166 | 101 |
| Si.Al.K.Fe_0 | 337 | unknown | 126 | 83 | 112 | 138 | 60 | 161 | 187 | 127 | 86 | 188 | 134 |
| Si.Al.Ca.Fe_1 | 307 | soil | 115 | 109 | 60 | 116 | 112 | 239 | 179 | 63 | 37 | 166 | 75 |
| Si.Al.K_2 | 272 | soil | 102 | 131 | 134 | 123 | 49 | 202 | 127 | 63 | 19 | 49 | 105 |
| Si.Al.Ca.Mg.Fe_1 | 266 | mineral | 99 | 138 | 78 | 119 | 67 | 187 | 116 | 67 | 37 | 130 | 52 |
| Si.Al_3 | 266 | soil | 99 | 54 | 37 | 179 | 41 | 213 | 179 | 63 | 37 | 58 | 131 |
| Si.Fe_4 | 247 | vehicle_industrial | 92 | 58 | 56 | 41 | 26 | 82 | 45 | 101 | 34 | 524 | 34 |
| Si.Al.Mg.K.Fe_1 | 235 | mineral | 88 | 173 | 75 | 78 | 60 | 146 | 105 | 41 | 37 | 36 | 105 |
| Si.Al_1 | 224 | soil | 84 | 125 | 52 | 90 | 52 | 246 | 86 | 41 | 26 | 49 | 56 |
| Si.Al.K.Fe_1 | 216 | soil | 81 | 96 | 56 | 78 | 34 | 157 | 112 | 49 | 49 | 49 | 119 |
| Si.Al.Fe_3 | 194 | brake | 72 | 42 | 26 | 75 | 49 | 149 | 71 | 131 | 37 | 112 | 45 |
| Si.Al_2 | 192 | soil | 72 | 32 | 26 | 112 | 30 | 194 | 146 | 45 | 45 | 31 | 56 |
| Ca.K_1 | 190 | biogenic | 71 | 80 | 149 | 183 | 101 | 7 | 7 | 4 | 105 | 40 | 26 |
| Si.Al.Na.Fe_1 | 190 | soil | 71 | 58 | 41 | 67 | 45 | 183 | 90 | 41 | 15 | 125 | 56 |
| Si.Al.Ca_2 | 187 | marl | 70 | 99 | 37 | 67 | 11 | 157 | 82 | 75 | 52 | 54 | 56 |
| Si.Al.Fe_4 | 176 | brake | 66 | 80 | 34 | 56 | 22 | 123 | 52 | 60 | 15 | 228 | 11 |

Appendix B. (cont.)

| | n | Source | AVG | DV1 | DV2 | DV3 | DV4 | DV5 | DV6 | U1 | U2 | U3 | PD |
|---|---|---|---|---|---|---|---|---|---|---|---|---|---|
| Si.Al.Mg.K.Fe_2 | 167 | mineral | 62 | 77 | 63 | 63 | 41 | 75 | 82 | 41 | 30 | 76 | 75 |
| Si.Al.Na.K_1 | 167 | mineral | 62 | 64 | 52 | 45 | 41 | 149 | 93 | 49 | 11 | 36 | 78 |
| Si.Al.Fe.S_1 | 158 | tire | 59 | 45 | 45 | 34 | 56 | 75 | 26 | 41 | 15 | 287 | 7 |
| Si.Al.K.Fe_4 | 154 | soil | 57 | 32 | 41 | 63 | 30 | 52 | 60 | 93 | 49 | 108 | 60 |
| Si.Al.K_1 | 144 | soil | 54 | 61 | 45 | 49 | 26 | 97 | 101 | 34 | 19 | 27 | 75 |
| Si.Al.Ca.K_2 | 137 | mineral | 51 | 90 | 75 | 52 | 52 | 26 | 49 | 11 | 26 | 76 | 52 |
| Si.K.Fe_1 | 128 | unknown | 48 | 13 | 34 | 49 | 49 | 60 | 63 | 52 | 67 | 54 | 45 |
| Si.Fe_3 | 125 | vehicle_industrial | 47 | 3 | 15 | 26 | 26 | 60 | 30 | 93 | 4 | 228 | 19 |
| Si.K.P_0 | 123 | unknown | 46 | 16 | 142 | 19 | 49 | 0 | 86 | 7 | 41 | 4 | 93 |
| Si.Fe_2 | 118 | vehicle_industrial | 44 | 16 | 19 | 34 | 41 | 19 | 67 | 78 | 19 | 139 | 30 |
| Si.Ca.Mg.Fe_1 | 114 | unknown | 43 | 74 | 34 | 52 | 22 | 34 | 52 | 30 | 37 | 67 | 22 |
| Si.Al.Na_0 | 107 | unknown | 40 | 35 | 11 | 52 | 49 | 75 | 52 | 30 | 22 | 27 | 45 |
| Ca_1 | 104 | calcite | 39 | 42 | 30 | 105 | 37 | 15 | 0 | 15 | 52 | 45 | 49 |
| Si.Al.K.P_0 | 104 | unknown | 39 | 19 | 101 | 11 | 7 | 4 | 142 | 4 | 7 | 4 | 86 |
| Si.Al.Mg.K.Fe_0 | 102 | unknown | 38 | 45 | 49 | 30 | 49 | 41 | 56 | 7 | 15 | 22 | 63 |
| K.P_1 | 99 | mineral | 37 | 0 | 131 | 26 | 41 | 0 | 30 | 0 | 56 | 0 | 86 |
| Si.Al.Mg.Fe_0 | 97 | unknown | 36 | 32 | 19 | 34 | 15 | 71 | 26 | 71 | 19 | 49 | 30 |
| Si.Al.Ca.Mg.K.Fe_1 | 96 | mineral | 36 | 96 | 34 | 19 | 34 | 34 | 22 | 4 | 15 | 76 | 22 |
| Si.Al.Fe_0 | 95 | unknown | 35 | 29 | 19 | 41 | 15 | 82 | 49 | 37 | 11 | 54 | 22 |
| Si.Al.Mg.Fe_1 | 95 | soil | 35 | 38 | 7 | 41 | 7 | 134 | 41 | 11 | 4 | 54 | 19 |
| Si.Ca.K_3 | 95 | mineral | 35 | 102 | 75 | 45 | 52 | 0 | 7 | 4 | 30 | 13 | 11 |
| Si.Fe_1 | 93 | mineral | 35 | 22 | 19 | 34 | 30 | 63 | 60 | 30 | 34 | 40 | 19 |
| K.Fe_0 | 90 | unknown | 34 | 0 | 30 | 26 | 15 | 4 | 11 | 49 | 11 | 63 | 138 |
| Si.Al.Ca.Fe_2 | 90 | soil | 34 | 51 | 49 | 49 | 19 | 71 | 45 | 15 | 7 | 22 | 4 |
| Si.Al.Ca.Na.Fe_1 | 90 | mineral | 34 | 45 | 22 | 34 | 7 | 82 | 30 | 19 | 15 | 90 | 0 |
| Si.Al.Ca.Fe_3 | 88 | marl | 33 | 26 | 19 | 34 | 22 | 56 | 34 | 56 | 11 | 54 | 22 |
| Si.Al.Ca.Mg.Fe_0 | 70 | unknown | 26 | 38 | 11 | 19 | 4 | 45 | 45 | 19 | 15 | 45 | 22 |
| Si.Al.Na.K.Fe_1 | 68 | mineral | 25 | 29 | 30 | 7 | 22 | 30 | 30 | 30 | 11 | 45 | 22 |
| Si.Al.Ca.Na.K_1 | 63 | mineral | 24 | 29 | 37 | 22 | 34 | 15 | 26 | 22 | 4 | 27 | 19 |

Appendix B. (cont.)

| | n | Source | AVG | DV1 | DV2 | DV3 | DV4 | DV5 | DV6 | U1 | U2 | U3 | PD |
|---|---|---|---|---|---|---|---|---|---|---|---|---|---|
| Si.Ca_3 | 60 | marl | 22 | 19 | 34 | 63 | 15 | 11 | 11 | 19 | 30 | 13 | 7 |
| Si.Al.K.Fe.S_1 | 57 | mineral | 21 | 32 | 41 | 4 | 30 | 4 | 19 | 30 | 7 | 40 | 7 |
| Si.K.S.P_0 | 57 | unknown | 21 | 29 | 71 | 7 | 34 | 0 | 22 | 0 | 41 | 0 | 4 |
| Si.Al.Ca.K.Fe_2 | 56 | soil | 21 | 45 | 26 | 4 | 30 | 19 | 19 | 7 | 15 | 13 | 26 |
| Si.Al.Ca.K.Fe_4 | 56 | mineral | 21 | 19 | 19 | 30 | 19 | 26 | 19 | 26 | 15 | 31 | 7 |
| Si.Al.K.S.P_0 | 51 | unknown | 19 | 38 | 49 | 7 | 15 | 0 | 52 | 7 | 4 | 0 | 11 |
| Si.Al.Ca.K.Fe_1 | 50 | soil | 19 | 29 | 34 | 19 | 26 | 19 | 26 | 0 | 7 | 9 | 15 |
| Si.Al.K.Fe.P_0 | 45 | unknown | 17 | 10 | 52 | 15 | 15 | 0 | 45 | 4 | 0 | 0 | 26 |
| Si.Ca.K_1 | 44 | mineral | 16 | 38 | 19 | 7 | 52 | 4 | 11 | 0 | 15 | 4 | 7 |
| Si.Al.Na.K_0 | 37 | unknown | 14 | 16 | 30 | 22 | 19 | 0 | 4 | 4 | 7 | 18 | 19 |
| Si.Al.Mg.Fe.S_0 | 36 | unknown | 13 | 16 | 7 | 7 | 4 | 45 | 4 | 15 | 7 | 31 | 0 |
| Si.Al.Ca_3 | 35 | marl | 13 | 6 | 11 | 34 | 11 | 7 | 7 | 26 | 7 | 9 | 11 |
| Ca.Fe_5 | 34 | vehicle_industrial | 13 | 3 | 0 | 0 | 22 | 0 | 0 | 34 | 0 | 22 | 49 |
| Si.Al.Ca.Fe.S_2 | 34 | mineral | 13 | 6 | 30 | 15 | 7 | 15 | 7 | 15 | 0 | 36 | 0 |
| Si.Al.Ca.Ti.Fe_1 | 34 | vehicle_industrial | 13 | 19 | 7 | 11 | 11 | 19 | 22 | 4 | 7 | 13 | 11 |
| Si.Al.Ca.K.Fe_5 | 33 | mineral | 12 | 19 | 15 | 11 | 11 | 11 | 11 | 0 | 11 | 9 | 22 |
| Ca.Fe_4 | 31 | vehicle_industrial | 12 | 0 | 4 | 0 | 11 | 0 | 0 | 34 | 0 | 27 | 45 |
| Si.K.Fe_0 | 31 | unknown | 12 | 0 | 7 | 11 | 11 | 0 | 4 | 19 | 11 | 40 | 19 |
| Si.Al.Ca.K.Fe_0 | 30 | unknown | 11 | 3 | 11 | 11 | 7 | 11 | 15 | 15 | 30 | 0 | 7 |
| Si.Ti.Fe_0 | 30 | unknown | 11 | 3 | 15 | 4 | 4 | 22 | 7 | 19 | 4 | 40 | 0 |
| Si.Al.Ca.K_1 | 29 | mineral | 11 | 13 | 4 | 4 | 11 | 22 | 22 | 4 | 4 | 13 | 11 |
| Si.Ca.Fe_3 | 29 | mineral | 11 | 3 | 7 | 7 | 4 | 15 | 4 | 15 | 19 | 22 | 15 |
| Si.Al.Ca_1 | 28 | marl | 10 | 13 | 19 | 15 | 15 | 11 | 11 | 4 | 0 | 13 | 4 |
| Si.Al.K.Fe.S.P_0 | 28 | unknown | 10 | 19 | 19 | 4 | 7 | 0 | 30 | 11 | 4 | 9 | 0 |
| Si.Ca_1 | 28 | marl | 10 | 35 | 4 | 0 | 11 | 7 | 7 | 0 | 7 | 27 | 4 |
| K.S.P_1 | 27 | mineral | 10 | 13 | 45 | 0 | 7 | 0 | 4 | 0 | 26 | 4 | 0 |
| Si.Al.Mg.K_0 | 27 | unknown | 10 | 0 | 26 | 15 | 7 | 15 | 7 | 4 | 0 | 9 | 19 |
| Si.Ca.Fe_5 | 27 | mineral | 10 | 16 | 0 | 4 | 4 | 4 | 0 | 11 | 7 | 63 | 0 |
| Si.K.S_0 | 27 | unknown | 10 | 13 | 4 | 4 | 7 | 0 | 11 | 11 | 41 | 4 | 4 |

| | n | Source | AVG | DV1 | DV2 | DV3 | DV4 | DV5 | DV6 | U1 | U2 | U3 | PD |
|---|---|---|---|---|---|---|---|---|---|---|---|---|---|
| Si.Al.Ca.Na_2 | 26 | mineral | 10 | 16 | 7 | 4 | 15 | 4 | 4 | 34 | 4 | 4 | 4 |
| Si.Al.Ca.Ti_1 | 26 | mineral | 10 | 19 | 7 | 0 | 11 | 26 | 15 | 0 | 4 | 13 | 0 |
| Si.Al.Mg.Na.Fe_0 | 26 | unknown | 10 | 19 | 15 | 15 | 0 | 26 | 4 | 4 | 0 | 9 | 4 |
| Si.Al.Ti.Fe_4 | 26 | brake | 10 | 19 | 0 | 7 | 4 | 19 | 15 | 4 | 0 | 27 | 4 |
| Al_1 | 25 | brake | 9 | 3 | 4 | 34 | 4 | 0 | 11 | 11 | 0 | 13 | 15 |
| Si.Al.Ca.Mg.Ti.Fe_0 | 25 | unknown | 9 | 6 | 4 | 11 | 7 | 34 | 7 | 0 | 0 | 22 | 4 |
| Si.Al.K_3 | 25 | unknown | 9 | 13 | 7 | 7 | 0 | 22 | 11 | 11 | 4 | 4 | 11 |
| Si.Al.Na.Fe_0 | 25 | unknown | 9 | 0 | 0 | 4 | 7 | 7 | 15 | 11 | 4 | 45 | 7 |
| Si.Ca_2 | 25 | marl | 9 | 16 | 7 | 26 | 7 | 0 | 11 | 4 | 0 | 9 | 11 |
| Si.Al.K.S_0 | 24 | unknown | 9 | 10 | 26 | 4 | 0 | 4 | 11 | 11 | 15 | 9 | 0 |
| Si.Al.K.Ti.Fe_0 | 23 | unknown | 9 | 0 | 7 | 19 | 4 | 19 | 4 | 15 | 4 | 9 | 7 |
| Si.Ca.Ti_1 | 23 | mineral | 9 | 10 | 7 | 4 | 0 | 26 | 4 | 7 | 4 | 13 | 11 |
| Si.P_2 | 23 | mineral | 9 | 0 | 4 | 41 | 11 | 0 | 11 | 0 | 7 | 0 | 11 |
| Si.Al.Fe.S_2 | 22 | tire | 8 | 10 | 0 | 7 | 4 | 0 | 11 | 4 | 0 | 54 | 0 |
| Si.Al.K.Ti.Fe_1 | 22 | unknown | 8 | 6 | 11 | 11 | 0 | 19 | 11 | 11 | 4 | 0 | 7 |
| Si.Ca.K.Fe_0 | 22 | unknown | 8 | 16 | 0 | 7 | 4 | 7 | 7 | 11 | 4 | 22 | 4 |
| Si.Mg.Fe_2 | 22 | mineral | 8 | 0 | 11 | 4 | 7 | 22 | 15 | 4 | 4 | 13 | 4 |
| P_1 | 21 | mineral | 8 | 0 | 4 | 41 | 7 | 0 | 4 | 0 | 7 | 4 | 11 |
| Si.Al.Ti.Fe_3 | 21 | mineral | 8 | 3 | 7 | 7 | 7 | 30 | 4 | 7 | 0 | 13 | 0 |
| Si.Al.Ca.K.Ti.Fe_0 | 20 | unknown | 7 | 13 | 0 | 4 | 4 | 11 | 7 | 11 | 7 | 13 | 4 |
| Si.Al.Ti.Fe_1 | 20 | mineral | 7 | 3 | 0 | 4 | 4 | 26 | 11 | 11 | 0 | 0 | 15 |
| Ti.Fe_2 | 20 | vehicle_industrial | 7 | 0 | 4 | 0 | 4 | 11 | 0 | 11 | 7 | 40 | 4 |
| Si.Mg.K.Fe_0 | 19 | unknown | 7 | 3 | 11 | 4 | 7 | 11 | 11 | 0 | 7 | 4 | 11 |
| Si.Al.Ca.Ti_3 | 18 | mineral | 7 | 6 | 11 | 11 | 4 | 15 | 7 | 0 | 4 | 9 | 0 |
| Si.Ca.Na_1 | 18 | mineral | 7 | 19 | 7 | 4 | 15 | 11 | 0 | 4 | 0 | 4 | 0 |
| Si.Al.Ca.K.Fe_3 | 17 | soil | 6 | 22 | 4 | 0 | 7 | 0 | 7 | 4 | 0 | 4 | 11 |
| Si.Al.Ca.K.S.P_0 | 17 | unknown | 6 | 29 | 7 | 0 | 4 | 0 | 7 | 0 | 7 | 0 | 4 |
| Si.Al.Ca.Na.K.Fe_0 | 17 | unknown | 6 | 6 | 11 | 0 | 7 | 4 | 4 | 11 | 0 | 18 | 4 |
| Si.Al.Ca.Ti.Fe_3 | 17 | vehicle_industrial | 6 | 3 | 4 | 4 | 0 | 15 | 15 | 4 | 11 | 9 | 0 |

Appendix B. (cont.)

| | n | Source | AVG | DV1 | DV2 | DV3 | DV4 | DV5 | DV6 | U1 | U2 | U3 | PD |
|---|---|---|---|---|---|---|---|---|---|---|---|---|---|
| Si.Al.Mg.K.Fe.P_0 | 17 | unknown | 6 | 10 | 22 | 0 | 4 | 0 | 15 | 0 | 0 | 0 | 11 |
| Si.Al.Mg.Ti.Fe_0 | 17 | unknown | 6 | 10 | 4 | 4 | 0 | 26 | 0 | 11 | 0 | 9 | 0 |
| K.S_2 | 16 | mineral | 6 | 0 | 19 | 4 | 4 | 0 | 4 | 7 | 15 | 4 | 4 |
| Si.Ca.Mg.K.Fe_0 | 16 | unknown | 6 | 3 | 11 | 11 | 7 | 7 | 0 | 0 | 7 | 9 | 4 |
| Si.Mg_1 | 16 | mineral | 6 | 6 | 0 | 4 | 0 | 7 | 0 | 0 | 34 | 4 | 4 |
| Ti_1 | 16 | vehicle_industrial | 6 | 3 | 0 | 4 | 11 | 4 | 4 | 15 | 0 | 4 | 15 |
| Si.Al.Ca.K.P_0 | 15 | unknown | 6 | 16 | 19 | 4 | 4 | 0 | 7 | 0 | 4 | 0 | 0 |
| Si.Al.Ti.Fe_0 | 15 | unknown | 6 | 6 | 4 | 7 | 7 | 11 | 0 | 7 | 0 | 13 | 0 |
| Si.Al.Mg_1 | 14 | mineral | 5 | 13 | 4 | 0 | 4 | 19 | 4 | 4 | 0 | 0 | 4 |
| Si.Al.Ti_2 | 14 | unknown | 5 | 10 | 0 | 4 | 4 | 22 | 0 | 7 | 0 | 4 | 0 |
| Ca.K.Fe_0 | 13 | unknown | 5 | 3 | 0 | 4 | 0 | 0 | 0 | 7 | 0 | 18 | 19 |
| Si.Al.Ca.K.Ti_0 | 13 | unknown | 5 | 0 | 11 | 11 | 4 | 7 | 4 | 4 | 0 | 4 | 4 |
| Si.Al.Fe.P_0 | 13 | unknown | 5 | 13 | 4 | 7 | 4 | 0 | 7 | 4 | 4 | 0 | 4 |
| Si.Al.Ti.Fe_2 | 13 | mineral | 5 | 6 | 0 | 11 | 0 | 15 | 4 | 4 | 4 | 4 | 0 |
| Ca.K.P_2 | 12 | mineral | 4 | 10 | 11 | 7 | 11 | 0 | 0 | 0 | 4 | 0 | 0 |
| Si.Al.Ca.K_3 | 12 | mineral | 4 | 6 | 4 | 0 | 4 | 7 | 4 | 7 | 0 | 9 | 4 |
| Si.Ca.Ti.Fe_2 | 12 | unknown | 4 | 0 | 0 | 0 | 0 | 7 | 11 | 4 | 7 | 18 | 0 |
| Ti.Fe_1 | 12 | vehicle_industrial | 4 | 3 | 0 | 4 | 15 | 0 | 0 | 11 | 4 | 4 | 4 |
| Al.Fe_3 | 11 | brake | 4 | 3 | 7 | 0 | 0 | 0 | 0 | 15 | 0 | 0 | 15 |
| Si.Al.Ca.K.Fe.S_1 | 11 | mineral | 4 | 3 | 4 | 0 | 11 | 4 | 4 | 0 | 7 | 9 | 0 |
| Si.Al.Ca.K_0 | 11 | unknown | 4 | 22 | 7 | 0 | 4 | 0 | 0 | 0 | 0 | 0 | 4 |
| Si.Al.K.Ti_0 | 11 | unknown | 4 | 6 | 0 | 4 | 15 | 4 | 0 | 7 | 0 | 4 | 0 |
| Si.Al.Mg.Na.K.Fe_0 | 11 | unknown | 4 | 6 | 4 | 0 | 4 | 4 | 7 | 7 | 0 | 4 | 4 |
| Si.Al.Na.K.Fe_0 | 11 | unknown | 4 | 3 | 0 | 7 | 4 | 4 | 4 | 7 | 0 | 9 | 4 |
| Si.Ca.Fe_1 | 11 | mineral | 4 | 3 | 7 | 4 | 4 | 4 | 4 | 7 | 0 | 9 | 0 |
| Si.Al.Fe.S_0 | 10 | tire | 4 | 3 | 4 | 0 | 7 | 4 | 7 | 4 | 0 | 9 | 0 |
| Si.Al.Mg.K.Ti.Fe_0 | 10 | unknown | 4 | 10 | 4 | 4 | 7 | 4 | 0 | 0 | 0 | 4 | 4 |
| Si.Al.P_0 | 10 | unknown | 4 | 0 | 4 | 7 | 7 | 4 | 11 | 4 | 0 | 0 | 0 |
| Si.Al_4 | 10 | soil | 4 | 0 | 0 | 15 | 4 | 4 | 7 | 4 | 0 | 0 | 4 |

Appendix B. (cont.)

| | n | Source | AVG | DV1 | DV2 | DV3 | DV4 | DV5 | DV6 | U1 | U2 | U3 | PD |
|---|---|---|---|---|---|---|---|---|---|---|---|---|---|
| Si.Al_5 | 10 | brake | 4 | 0 | 0 | 15 | 4 | 7 | 7 | 0 | 4 | 0 | 0 |
| Si.Ca.K.S.P_1 | 10 | mineral | 4 | 19 | 7 | 0 | 4 | 0 | 0 | 0 | 4 | 0 | 0 |
| Si.Mg.K_0 | 10 | unknown | 4 | 3 | 0 | 4 | 4 | 4 | 7 | 4 | 0 | 4 | 7 |
| Si.S_2 | 10 | mineral | 4 | 6 | 0 | 7 | 0 | 0 | 7 | 4 | 4 | 4 | 4 |
| Si.Ti.Fe_2 | 10 | unknown | 4 | 0 | 7 | 4 | 0 | 7 | 4 | 4 | 0 | 13 | 0 |